Computer Methods in Applied Mechanics and Engineering 421 (2024) 116792

Contents lists available at ScienceDirect

Comput. Methods Appl. Mech. Engrg.

journal homepage: www.elsevier.com/locate/cma

Moment-based, univariate n-point quadrature rules in application to the full network model of rubber elasticity

Ben R. Britt, Alexander E. Ehret *

Empa, Swiss Federal Laboratories for Materials Science and Technology, Überlandstrasse 129, CH-8600, Dübendorf, Switzerland
ETH Zurich, Institute for Mechanical Systems, Leonhardstrasse 21, CH-8092, Zürich, Switzerland

ARTICLE INFO

Keywords:
Spherical cubature
Statistical moments
Stretch distribution
Multiscale modelling
Full network
Affine deformation

ABSTRACT

In this contribution we provide numerical methods to implement full network models with particular application to affine isotropic networks as they are frequently applied in theories of rubber elasticity. Unlike the common approaches, the average of the single chains' responses is not obtained by spherical integration but by solving a univariate integral expressed in terms of the squared stretch of a fibre's or chain's end-to-end vector. In addition to the free energy function of these individual elements the methods are informed by the statistical moments of the distribution of stretch in the network, which throughout the work is assumed to be determined by affine kinematics. We exemplify the proposed procedure for two quadrature methods, which distinguish in terms of the positions of the n integration points and the corresponding weights. While the first method uses constant equal weights of $1/n$ and hence only requires the computation of n integration points, the second, Gauss-type method also requires the determination of the corresponding weights and builds on a recent development, previously implemented for up to 3 points (Britt & Ehret, *Comput. Methods Appl. Mech. Engrg.* 415, 2023). However, the structure of the solution strategy applies to a wider range of univariate quadrature rules. Both methods exemplified here can be made exact for polynomial chain free energy functions of arbitrary order, and are illustrated in application to the affine full network model of rubber elasticity with non-Gaussian chains. The results indicate high accuracy of the new methods and therefore identify them as useful and efficient alternatives to the existing approaches for computing the full network response.

1. Introduction

In continuum mechanical theories of materials whose structure at smaller length-scales consists of a network of fibres or long molecules, the macroscopic mechanical response is often obtained as an average of the responses elicited by these single elements. In general, such approaches require a relation between the kinematics at the macroscale, at which the material can be assumed to obey the physical laws of a continuous solid, and the microscale kinematics. We have recently proposed to establish this relation in a probabilistic manner by describing the distribution of microscopic stretch within the network [1], whereas the way more common approach uses an intermediate step, in that the stretch of an element is first related to its referential orientation, and the average is evaluated as an integral over the orientation distribution. Since the set of possible orientations in d dimensions can be associated with the unit sphere $\mathcal{S}_{d-1}$, the integrals are typically evaluated on $\mathcal{S}_{d-1}$.

* Corresponding author at: Empa, Swiss Federal Laboratories for Materials Science and Technology, Überlandstrasse 129, CH-8600, Dübendorf, Switzerland.
E-mail addresses: ben-rudolf.britt@empa.ch (B.R. Britt), alexander.ehret@empa.ch (A.E. Ehret).

https://doi.org/10.1016/j.cma.2024.116792
Received 6 September 2023; Received in revised form 15 January 2024; Accepted 19 January 2024
Available online 31 January 2024

Several important applications in continuum mechanics employ affine modelling concepts such as the affine full network of rubber elasticity [2,3] or the structural approach in soft tissue biomechanics [4–8], i.e. fibres are assumed to transform like vectorial line elements of a continuous body. In Britt and Ehret [9], we have elaborated the affine stretch distribution corresponding to a referential orientation distribution and a given macroscopic state of deformation, and showed that the stretch distribution approach [1] also applies in the affine case, thereby generalising results in previous work [10,11]. Particularly, we highlighted that this approach suggests several alternative methods to implement affine modelling concepts. One of the key features of the alternative interpretation of the average in terms of the stretch distribution concerns the dimensionality of the probability space: The alternative form only requires integration over the range of admissible stretches, which is the set of positive reals in the general case, and the bounded interval between the extremal principal stretches in the affine case. Very effective numerical integration schemes exist for such univariate integrals, and following the concept of moment-preserving integration schemes [12,13] we proposed the use of Gauss quadrature (GI) in Britt and Ehret [14], illustrated for the important special case of structural models for anisotropic soft tissues. Strikingly, it was shown that already a 3-point scheme, for which the integration points and weights can be determined analytically, can compete with high-order spherical integration schemes and is even superior with regard to preserving material symmetry [14]. Like in most of the alternatives proposed to circumvent spherical cubature [e.g. 10,15–18], the method uses higher order structural tensors [19,20], to include information about the material's anisotropy. Although the latter can be computed and stored very efficiently [14,21], their tensorial order, increasing with the number n of Gauss integration points as $2(2n-1)$, may still set limits on what one would use during the computations. Notably, this is different in the isotropic case, where the moments are only functions of the right Cauchy–Green tensor, and the problem reduces to efficient methods for calculating integration points and weights.

Hence, after introducing a second quadrature scheme (EWI) with a set of constant, equal weights, a practical numerical framework is proposed in the present work, to determine the positions of the integration points for such moment-preserving quadratures, so that they can be implemented to be exact for polynomials of arbitrary order.

This extension is of particular relevance in fields where the constitutive behaviour of the fibres is characterised by very high non-linearity. Therefore the proposed n-point GI and EWI quadrature rules are illustrated for a second prime example of network averaging: the affine full network model of non-Gaussian elasticity [2], whose efficient implementation has been subject of research over several decades [e.g. 22–28]. Most expressions for the free energy of non-Gaussian chains reflect the property of limited chain extensibility, i.e. they diverge as the chain's end-to-end stretch approaches the fully extended length [29,30], and are hence non-analytic in this region. For the isotropic full network model there exists already a powerful analytical method based on a Taylor series expansion (TE) of the free energy of a single non-Gaussian polymer chain [27], which allows expressing the network free energy as a weighted sum of terms which themselves are functions of the principal invariants. It was shown that these terms correspond to statistical moments of the affine distribution [9], i.e. integrals of integer powers over the affine stretch distribution. Although the here proposed methods likewise make use of these moments, they are employed differently: Requiring their preservation in numerical integration, they serve to identify the positions of integration points of univariate quadrature schemes. For different implementations of the non-Gaussian chain [2,31,32] we obtain very accurate results of the full network model in the typical range of interest for both proposed quadrature methods. Their results approach the ground truth with increasing n for both GI and EWI. The comparison of the existing TE method with GI and EWI using the same number of statistical moments suggests that the new methods use this information more efficiently.

The paper is organised as follows: Section 2 provides some technical preliminaries and resumes the idea of computing averages from the distribution of stretch – square stretch to be precise. Section 3 outlines the concept of univariate moment-preserving quadratures to integrate full network models, resumes the Gauss-type rule [14] and, as another member of this family, introduces a quadrature with equal weights. In Section 4 we derive the numerical treatment of the Gauss and equal weights quadrature rules for arbitrary n. Section 5 is dedicated to different implementations of the full-network model of rubber elasticity. The results are presented and discussed in Section 6, and the paper is concluded in Section 7.

2. Preliminaries

2.1. Continuum mechanics fundamentals

The deformation of a material body is described by the mapping $\boldsymbol{\varphi} : \mathcal{B}_0 \to \mathcal{B}_t, \boldsymbol{X} \mapsto \boldsymbol{x}$, taking a material point from its position $\boldsymbol{X}$ in the reference configuration $\mathcal{B}_0$ to its current position $\boldsymbol{x}$ in the current configuration $\mathcal{B}_t$. The corresponding deformation gradient is $\mathbf{F} = \partial\boldsymbol{\varphi}/\partial\boldsymbol{X}$ with determinant $J = \det\mathbf{F} > 0$, and allows to define the right Cauchy–Green tensor as $\mathbf{C} = \mathbf{F}^{\mathrm{T}}\mathbf{F}$.

Let the free energy Ψ per unit reference volume be given by the function $\hat{\Psi} : \mathbf{C} \mapsto \Psi$. For a hyperelastic unconstrained material the second Piola–Kirchhoff stress $\mathbf{S}$, the related first Piola–Kirchhoff stress $\mathbf{P}$ and Cauchy stress $\boldsymbol{\sigma}$ as well as fourth-order tangent tensor $\mathbb{C}$ are obtained as

$$\mathbf{S} = 2\frac{\partial\hat{\Psi}}{\partial\mathbf{C}}, \quad \mathbf{P} = \mathbf{F}\mathbf{S}, \quad \boldsymbol{\sigma} = J^{-1}\mathbf{F}\mathbf{S}\mathbf{F}^{\mathrm{T}}, \quad \mathbb{C} = 2\frac{\partial\mathbf{S}}{\partial\mathbf{C}} = 4\frac{\partial^2\hat{\Psi}}{\partial\mathbf{C}\partial\mathbf{C}}. \tag{1}$$

We assume that the reference configuration $\mathcal{B}_0$ is associated with an energy- and stress-free state of the material, i.e. $\hat{\Psi}(\mathbf{I}) = 0$ and $\mathbf{S}(\mathbf{I}) = \mathbf{0}$.

2.2. Tensor algebra and analysis fundamentals

Let $\mathbf{T}$ be a generally non-symmetric 2nd order tensor. The *principal traces* of $\mathbf{T}$ read

$$J_1 = \mathrm{tr}\mathbf{T}, \quad J_2 = \mathrm{tr}\mathbf{T}^2, \quad J_3 = \mathrm{tr}\mathbf{T}^3, \quad \dots, \quad J_d = \mathrm{tr}\mathbf{T}^d, \tag{2}$$

and are also referred to as *main invariants* of $\mathbf{T}$. They are equivalently expressed in terms of its eigenvalues $\{\lambda_k\}$ as

$$\begin{aligned} J_1 &= \lambda_1 + \lambda_2 + \lambda_3 + \dots + \lambda_d, \\ J_2 &= \lambda_1^2 + \lambda_2^2 + \lambda_3^2 + \dots + \lambda_d^2, \\ J_3 &= \lambda_1^3 + \lambda_2^3 + \lambda_3^3 + \dots + \lambda_d^3, \\ &\vdots \\ J_d &= \lambda_1^d + \lambda_2^d + \lambda_3^d + \dots + \lambda_d^d, \end{aligned} \tag{3}$$

and are related to the *principal invariants* through Newton's identities [see e.g. 33], such that

$$\begin{aligned} I_1 &= J_1, \\ I_2 &= \frac{1}{2}(I_1 J_1 - J_2), \\ I_3 &= \frac{1}{3}(I_2 J_1 - I_1 J_2 + J_3), \\ &\vdots \\ I_d &= \frac{1}{d}(I_{d-1} J_1 - I_{d-2} J_2 + \dots + (-1)^{d-1} J_d) = \det\mathbf{T}. \end{aligned} \tag{4}$$

The case where $\mathbf{T}$ has d distinct eigenvalues $\{\lambda_k\}$, is particularly relevant to this work, and in this case [e.g. 33]

$$\mathbf{T} = \sum_{k=1}^{d} \lambda_k \mathbf{P}_k, \tag{5}$$

where $\{\mathbf{P}_l\}$ are the corresponding eigenprojections. In this case, one can show that the derivatives of the eigenvalues with respect to $\mathbf{T}$ are [33, Sec. 6]

$$\lambda_{k,\mathbf{T}} = \lambda_k \mathbf{P}_k^{\mathrm{T}} \quad \text{(no sum over } k\text{)}, \tag{6}$$

and the derivatives of the eigenprojections with respect to (non-symmetric) $\mathbf{T}$ are [33, Sec. 7]

$$\mathbf{P}_{k,\mathbf{T}} = \sum_{\substack{l=1 \\ l \neq k}}^{d} \frac{\mathbf{P}_k \boxdot \mathbf{P}_l + \mathbf{P}_l \boxdot \mathbf{P}_k}{\lambda_k - \lambda_l} \quad \text{(no sum over } k\text{)}, \tag{7}$$

where the tensor product $\boxdot$ between the 2nd order tensors $\mathbf{A}$ and $\mathbf{B}$ is defined such that

$$\mathbf{A} \boxdot \mathbf{B} : \mathbf{X} = \mathbf{A}\mathbf{X}\mathbf{B} \tag{8}$$

for all 2nd order tensors $\mathbf{X}$. We note that in case $\mathbf{T}$ is symmetric, instead of $\boxdot$ one may use the (partly) symmetrised product $\boxtimes$ defined such that [cp. e.g. 9]

$$\mathbf{A} \boxtimes \mathbf{B} : \mathbf{X} = \mathbf{A}(\mathbf{X} + \mathbf{X}^{\mathrm{T}})/2\,\mathbf{B}. \tag{9}$$

The definitions given within this section can also be interpreted analogously for matrices $\mathsf{T} \in \mathbb{R}^{d\times d}$ or $\mathbb{C}^{d\times d}$. This becomes particularly evident if we consider the tensors to be represented with respect to a fixed orthonormal basis, so that Eqs. (2)–(9) operate on their Cartesian components. We will exploit this circumstance in the next section.

2.3. Polynomials and companion matrices

The problem of finding the n zeros $\{\bar{\xi}_k\}$ of a monic polynomial (polynomial with leading coefficient 1), i.e. the solutions of

$$\bar{\xi}^n + a_{n-1}\bar{\xi}^{n-1} + a_{n-2}\bar{\xi}^{n-2} + \dots + a_0 = 0, \tag{10}$$

is equivalent to finding the eigenvalues of the $n \times n$ companion matrix M, defined by [cf. 34,35]

$$\mathsf{M} = \begin{bmatrix} 0 & 0 & \dots & 0 & -a_0 \\ 1 & 0 & \dots & 0 & -a_1 \\ 0 & 1 & \dots & 0 & -a_2 \\ \vdots & \vdots & \ddots & \vdots & \vdots \\ 0 & 0 & \dots & 1 & -a_{n-1} \end{bmatrix}. \tag{11}$$

The computation of the eigenvalues $\{\bar{\xi}_k\}$ and a set of corresponding n-dimensional eigenvectors $\{\mathsf{v}_k\}$ of M is a standard task accomplished by linear algebra packages in a variety of programming languages.

Assuming the roots of the polynomial (10) and thus the eigenvalues of M (11) are distinct, it follows that M is diagonalisable, i.e. [cf. e.g. 34]

$$\mathsf{V}^{-1}\mathsf{M}\mathsf{V} = \operatorname{diag}\{\bar{\xi}_k\} \iff \mathsf{M} = \mathsf{V}\operatorname{diag}\{\bar{\xi}_k\}\,\mathsf{V}^{-1}, \tag{12}$$

where the n columns of V represent the n eigenvectors v_k of M, so that it is obtained by concatenating the n vectors as

$$\mathsf{V} = \begin{bmatrix}\mathsf{v}_1 & \mathsf{v}_2 & \dots & \mathsf{v}_n\end{bmatrix}. \tag{13}$$

Instead of using an arbitrary set of eigenvectors, we remark that another possible choice for the transformation matrix is to set $\mathsf{V}^{-\mathrm{T}}$ equal to the Vandermonde matrix [cf. e.g. 34, Sec. 3.3.P20]

$$\mathsf{V}^{-\mathrm{T}} = \begin{bmatrix} 1 & 1 & 1 & \dots & 1 \\ \bar{\xi}_1 & \bar{\xi}_2 & \bar{\xi}_3 & \dots & \bar{\xi}_n \\ \bar{\xi}_1^2 & \bar{\xi}_2^2 & \bar{\xi}_3^2 & \dots & \bar{\xi}_n^2 \\ \vdots & \vdots & & \vdots & \\ \bar{\xi}_1^{n-1} & \bar{\xi}_2^{n-1} & \bar{\xi}_3^{n-1} & \dots & \bar{\xi}_n^{n-1} \end{bmatrix}. \tag{14}$$

The diagonalisation (12) implies that the n^2 components of M can be represented as

$$\mathsf{M}_{\alpha\beta} = \sum_{k=1}^{n} \bar{\xi}_k \mathsf{V}_{\alpha k}\mathsf{V}^{-1}_{k\beta} = \sum_{k=1}^{n} \bar{\xi}_k (\mathsf{P}_k)_{\alpha\beta}, \tag{15}$$

where the matrices $\{\mathsf{P}_k\}$, obtained by matrix multiplication of the kth column of V with the kth row of V^{-1}, take the role of eigenprojections, in analogy to Eq. (5). Hence, in analogy to Eqs. (6),(7) one finds

$$(\bar{\xi}_k)_{,\mathsf{M}_{\alpha\beta}} = (\mathsf{P}_k)_{\beta\alpha} \tag{16}$$

and

$$(\mathsf{P}_k)_{\alpha\beta,\mathsf{M}_{\gamma\delta}} = \sum_{\substack{l=1 \\ l\neq k}}^{d} \frac{(\mathsf{P}_k)_{\alpha\gamma}(\mathsf{P}_l)_{\delta\beta} + (\mathsf{P}_l)_{\alpha\gamma}(\mathsf{P}_k)_{\delta\beta}}{\bar{\xi}_k - \bar{\xi}_l}. \tag{17}$$

2.4. Integration of the fibre energy

We propose a method to approximate or define the macroscopic free energy Ψ of the fibre network from a fibre strain–energy (density) function ψ of the affine fibre square stretch Λ. To this end, we introduce the expectation operator $\mathrm{E}[\,\cdot\,]$, for which $\mathrm{E}[1] = 1$, to express the macroscopic energy Ψ as an integral of the microscopic energy ψ, i.e.

$$\Psi = \nu\,\mathrm{E}[\psi] - C, \tag{18}$$

where ν is a constant for the energetic scale equivalence [1] and C is a constant[1] to guarantee an energy-free reference state. If we limit our attention to the isotropic affine case, the integral $\mathrm{E}[\psi]$ can be given by

$$\mathrm{E}[\psi] = \frac{1}{4\pi}\int_S \psi(\mathbf{C} : \boldsymbol{N}\otimes\boldsymbol{N})\,\mathrm{d}A, \tag{19}$$

where $\mathbf{C} : \boldsymbol{N}\otimes\boldsymbol{N} = \|\mathbf{F}\boldsymbol{N}\|^2$ is the affine square stretch Λ of a line element initially oriented in direction with unit normal $\boldsymbol{N}$ and $\mathrm{d}A$ is the surface element of the sphere corresponding to $\boldsymbol{N}$. As it is convenient to parameterise the argument of the integral, e.g. $\boldsymbol{N}$, by spherical angles ϕ and θ we note that

$$\mathrm{E}[\,\cdot\,] = \frac{1}{4\pi}\int_S \cdot\,\mathrm{d}A = \frac{1}{4\pi}\int_0^{2\pi}\int_0^{\pi} \cdot\,\sin(\theta)\mathrm{d}\theta\,\mathrm{d}\phi. \tag{20}$$

As elaborated in Britt and Ehret [1], more generally, and particularly not requiring the existence of a relation between Λ and $\boldsymbol{N}$, the averaged macroscopic energy can be expressed in terms of the stretch distribution P_Λ for a given deformation

$$\mathrm{E}[\psi] = \int_0^\infty \psi(\xi)\,\mathrm{d}P_\Lambda(\xi), \tag{21}$$

or in terms of its density p_Λ (if this exists)

$$\mathrm{E}[\psi] = \int_0^\infty \psi(\xi)\,p_\Lambda(\xi)\,\mathrm{d}\xi. \tag{22}$$

For later use let us further introduce the raw $\{\mu_k\}$ and central moments $\{\bar{\mu}_k\}$ of the affine square stretch Λ [9]

$$\mu_k = \mathrm{E}\left[\Lambda^k\right], \quad \bar{\mu}_k = \mathrm{E}\left[(\Lambda - \mu_1)^k\right]. \tag{23}$$

[1] Particularly for entropic elasticity of polymer chains it is common to associate C with the free energy of the network in the reference state. Due to the potential character of Ψ this constant does not affect the calculation of stress.

2.5. Moments of the isotropic affine stretch distribution and their derivatives

In the isotropic affine case, one has

$$\mu_1 = \frac{1}{3} I_1 \tag{24}$$

and the first 30 central moments $\{\bar{\mu}_k\}$ computed using the algorithm provided in [9] are given in Appendix A (Table A.1) as polynomials of two dedicated invariants [cf. 9,27]

$$A = I_1^2 - 3I_2 = \frac{3}{2}\mathrm{tr}(\mathbf{C} - \mu_1\mathbf{I})^2, \qquad B = I_1^3 - \frac{9}{2} I_1 I_2 + \frac{27}{2} I_3 = \frac{27}{2}\det(\mathbf{C} - \mu_1\mathbf{I}). \tag{25}$$

For the differentiation of the moment-dependent expressions, that will be useful later, we further note [cf. 9]

$$A_{,\mathbf{C}} = 3\,(\mathbf{C} - \mu_1\mathbf{I}), \quad A_{,\mathbf{CC}} = 3\,\mathbf{I}\boxtimes\mathbf{I} - \mathbf{I}\otimes\mathbf{I} \tag{26}$$

and

$$\begin{aligned} B_{,\mathbf{C}} &= \frac{27}{2}\mathbf{adj}(\mathbf{C} - \mu_1\mathbf{I}) + \frac{3}{2} A\,\mathbf{I} = \frac{27}{2}(\mathbf{C} - \mu_1\mathbf{I})^2 - 3A\mathbf{I}, \\ B_{,\mathbf{CC}} &= \frac{27}{2}\left((\mathbf{C} - \mu_1\mathbf{I})\boxtimes\mathbf{I} + \mathbf{I}\boxtimes(\mathbf{C} - \mu_1\mathbf{I})\right) - 3(A_{,\mathbf{C}}\otimes\mathbf{I} + \mathbf{I}\otimes A_{,\mathbf{C}}), \end{aligned} \tag{27}$$

where the adjugate $\mathbf{adjA}$ of the 2nd order tensor $\mathbf{A}$, satisfying

$$\mathbf{adjA}\,\mathbf{A} = \det\mathbf{A}\,\mathbf{I}, \tag{28}$$

is used.

3. Univariate quadrature rules

The integral (21) can be computed by univariate quadrature rules as

$$\mathrm{E}[\psi] = \int_0^\infty \psi(\xi)\,\mathrm{d}P_\Lambda(\xi) \approx \mathrm{NQ}[\psi] = \sum_{k=1}^{n} \psi(\xi_k)\,\omega_k, \tag{29}$$

where NQ stands for any suitable numerical quadrature procedure, able to exactly integrate polynomial functions of a desired degree. The quadrature is characterised by n integration points ξ_k at which the integrand is evaluated, and corresponding weights ω_k.

To determine the positions of integration points and weights, we define a root-finding problem of the form (10) with coefficients $a_k = \hat{a}_k(\bar{\mu}_2, \bar{\mu}_3, \dots, \bar{\mu}_n)$, $k = 1, 2, \dots, n$. This procedure is intrinsic to the moment-based Gauss quadrature discussed in [14], where the integration points are the roots of orthogonal polynomials, as shown in Section 3.1. However, other strategies for integration can be brought to a suitable form, as exemplified for a quadrature rule with equal weights in Section 3.2.

3.1. Univariate Gauss quadrature

We have recently applied the Gauss quadrature rule to integrate the fibre strain–energy of an affinely deforming material with a continuous, generally non-uniform fibre orientation distribution. The univariate Gauss quadrature approximates [14]

$$\mathrm{E}[\psi] = \int_0^\infty \psi(x)\,\mathrm{d}P_\Lambda(x) \approx \mathrm{GI}[\psi] = \sum_{k=1}^{n} \psi(x_k) w_k. \tag{30}$$

The integration points ξ_k, referred to as x_k for GI,

$$x_k = \bar{x}_k + \mu_1 \tag{31}$$

result from the roots $\bar{x}_k$ of the nth orthogonal polynomial Q_n, and the corresponding weights $\{w_k\}$ compute as [see e.g. 36]

$$w_k = \mathrm{E}\left[\prod_{l\neq k} \frac{\bar{x} - \bar{x}_l}{\bar{x}_k - \bar{x}_l}\right], \quad k = 1, 2, \dots, n. \tag{32}$$

The Gauss quadrature has the following properties [see e.g. 36]: (i) The integration points are real, mutually distinct and lie within the stretch range, i.e. $x_k \in [\Lambda_{\min}, \Lambda_{\max}]$ (Supplementary Information, Sec. 1). (ii) The weights are positive, and (iii) the rule integrates polynomials up to degree $2n - 1$ exactly.

The nth orthogonal polynomial Q_n is expressed by the determinant formula [37]

$$Q_n = \begin{vmatrix} 1 & 0 & \bar{\mu}_2 & \bar{\mu}_3 & \dots & \bar{\mu}_n \\ 0 & \bar{\mu}_2 & \bar{\mu}_3 & \bar{\mu}_4 & \dots & \bar{\mu}_{n+1} \\ \bar{\mu}_2 & \bar{\mu}_3 & \bar{\mu}_4 & \bar{\mu}_5 & \dots & \bar{\mu}_{n+2} \\ \vdots & & & & & \vdots \\ \bar{\mu}_{n-1} & \bar{\mu}_n & \bar{\mu}_{n+1} & \bar{\mu}_{n+2} & \dots & \bar{\mu}_{2n-1} \\ 1 & \bar{x} & \bar{x}^2 & \bar{x}^3 & \dots & \bar{x}^n \end{vmatrix} \tag{33}$$

to be understood as a cofactor expansion of the $(n+1)\times(n+1)$ matrix along the last row, so that

$$\begin{aligned} Q_n = &\underbrace{\begin{vmatrix} 1 & 0 & \cdots & \bar{\mu}_{n-1} \\ 0 & \bar{\mu}_2 & \cdots & \bar{\mu}_n \\ \vdots & \vdots & \ddots & \vdots \\ \bar{\mu}_{n-1} & \bar{\mu}_n & \cdots & \bar{\mu}_{2n-2} \end{vmatrix}}_{c_n = \det \mathsf{A}_n} \bar{x}^n + (-1) \underbrace{\begin{vmatrix} 1 & \cdots & \bar{\mu}_{n-2} & \bar{\mu}_n \\ 0 & \cdots & \bar{\mu}_{n-1} & \bar{\mu}_{n-1} \\ \vdots & \ddots & \vdots & \vdots \\ \bar{\mu}_{n-1} & \cdots & \bar{\mu}_{2n-3} & \bar{\mu}_{2n-1} \end{vmatrix}}_{c_{n-1} = \det \mathsf{A}_{n-1}} \bar{x}^{n-1} + \cdots \\ &+ (-1)^{n-1} \underbrace{\begin{vmatrix} 1 & \bar{\mu}_2 & \cdots & \bar{\mu}_n \\ 0 & \bar{\mu}_3 & \cdots & \bar{\mu}_{n-1} \\ \vdots & \vdots & \ddots & \vdots \\ \bar{\mu}_{n-1} & \bar{\mu}_{n+1} & \cdots & \bar{\mu}_{2n-1} \end{vmatrix}}_{c_1 = \det \mathsf{A}_1} \bar{x} + (-1)^n \underbrace{\begin{vmatrix} 0 & \cdots & \bar{\mu}_{n-1} & \bar{\mu}_n \\ \bar{\mu}_2 & \cdots & \bar{\mu}_n & \bar{\mu}_{n-1} \\ \vdots & \ddots & \vdots & \vdots \\ \bar{\mu}_n & \cdots & \bar{\mu}_{2n-2} & \bar{\mu}_{2n-1} \end{vmatrix}}_{c_0 = \det \mathsf{A}_0} \bar{x}^0 = \sum_{k=0}^{n} c_k \, \bar{x}^k = \sum_{k=0}^{n} \bar{x}^k \det \mathsf{A}_k \,. \end{aligned} \tag{34}$$

Division by c_n yields the root finding problem of a monic polynomial of the form (10) as

$$\boxed{\bar{x}^n + \frac{c_{n-1}}{c_n} \bar{x}^{n-1} + \cdots + \frac{c_1}{c_n} \bar{x} + \frac{c_0}{c_n} = 0.} \tag{35}$$

The calculation of stress and elasticity tensors according to Eq. (1) from the network strain–energy (18) requires derivatives with respect to $\mathbf{C}$, and when approximated by the Gauss rule (30) the first and second ones read

$$\mathrm{GI}\,[\psi]_{,\mathbf{C}} = \sum_{k=1}^{n} \left[\psi'(x_k) w_k x_{k,\mathbf{C}} + \psi(x_k) w_{k,\mathbf{C}} \right], \tag{36}$$

and

$$\mathrm{GI}\,[\psi]_{,\mathbf{CC}} = \sum_{k=1}^{n} \left[\psi''(x_k) w_k \, x_{k,\mathbf{C}} \otimes x_{k,\mathbf{C}} + \psi(x_k) \, w_{k,\mathbf{CC}} \; + \psi'(x_k) \, \left(x_{k,\mathbf{C}} \otimes w_{k,\mathbf{C}} + w_{k,\mathbf{C}} \otimes x_{k,\mathbf{C}} \right) + \psi'(x_k) w_k \, x_{k,\mathbf{CC}} \right], \tag{37}$$

where $\otimes$ denotes the 'usual' tensor product between two second order tensors $\mathbf{A}, \mathbf{B}$ such that $\mathbf{A} \otimes \mathbf{B} : \mathbf{X} = \mathbf{A}(\mathbf{B} : \mathbf{X})$.

In Britt and Ehret [14] we have provided analytic expressions for $x_{k,\mathbf{C}}$, $w_{k,\mathbf{C}}$ as well as $x_{k,\mathbf{CC}}, w_{k,\mathbf{CC}}$ for the cases $n \leq 3$, for which the (up to) three roots x_1, x_2, x_3 can be determined analytically; an implementation can be found in [38].

3.2. Univariate equal weights quadrature

As an alternative to the Gauss quadrature (30) we propose to approximate the integral (21) by an n-point quadrature rule with equal weights $\omega_k = 1/n$ of the form

$$\mathrm{E}\,[\psi] \approx \mathrm{EWI}\,[\psi] = \frac{1}{n} \sum_{k=1}^{n} \psi(z_k), \tag{38}$$

where $\{z_k\}$ are the specific integration points $\{\xi_k\}$ for the EWI. As common in many integration schemes we determine $\{z_k\}$ such that the approximation (38) is exact for a polynomial ψ of degree n. An exact Taylor series representation of such a polynomial ψ reads

$$\psi = \sum_{l=0}^{n} \frac{1}{l!} \frac{\partial^l \psi}{\partial \Lambda^l} \bigg|_{\Lambda = \Lambda_0} (\Lambda - \Lambda_0)^l. \tag{39}$$

Inserting (39) into (38), one finds

$$\sum_{l=0}^{n} \frac{1}{l!} \frac{\partial^l \psi}{\partial \Lambda^l} \bigg|_{\Lambda = \Lambda_0} \mathrm{E}\left[(\Lambda - \Lambda_0)^l \right] \approx \frac{1}{n} \sum_{k=1}^{n} \sum_{l=0}^{n} \frac{1}{l!} \frac{\partial^l \psi}{\partial \Lambda^l} \bigg|_{\Lambda = \Lambda_0} (z_k - \Lambda_0)^l, \tag{40}$$

and as in this case full equivalence is required, by comparison of the coefficients it can be concluded that

$$\mathrm{E}\left[(\Lambda - \Lambda_0)^l \right] = \frac{1}{n} \sum_{k=1}^{n} (z_k - \Lambda_0)^l, \quad l = 0, 1, \ldots, n, \tag{41}$$

where for $l = 0$ the normalisation condition $\mathrm{E}\,[1] = 1$ is automatically satisfied as each weight is $1/n$. The choice of Λ_0 does not affect the result and therefore can be considered arbitrary, as long as it is real and positive. In Britt and Ehret [9] we have studied the distribution of the square stretch Λ in the affine model and identified the expressions $\mathrm{E}\left[(\Lambda - \Lambda_0)^l \right]$ as the lth moment of Λ with respect to Λ_0. If one chooses Λ_0 as the expectation or first (raw) moment μ_1 one finds the central moments $\{\bar{\mu}_l\}$.

With this choice ($\Lambda_0 = \mu_1$) Eq. (41) leads to the fundamental requirement on the n-point rule

$$\begin{aligned}
&\bar{z}_1 + \bar{z}_2 + \bar{z}_3 + \ldots + \bar{z}_n = 0\\
&\bar{z}_1^2 + \bar{z}_2^2 + \bar{z}_3^2 + \ldots + \bar{z}_n^2 = n\,\bar{\mu}_2\\
&\bar{z}_1^3 + \bar{z}_2^3 + \bar{z}_3^3 + \ldots + \bar{z}_n^3 = n\,\bar{\mu}_3\\
&\qquad\qquad\vdots\\
&\bar{z}_1^n + \bar{z}_2^n + \bar{z}_3^n + \ldots + \bar{z}_n^n = n\,\bar{\mu}_n,
\end{aligned} \tag{42}$$

where for the sake of brevity we have set

$$\bar{z}_k = z_k - \mu_1. \tag{43}$$

For the isotropic case the moments μ_1 and $\{\bar{\mu}_l\}$ are discussed in Section 2.5.

The formal comparison of Eq. (42) with Eq. (3) reveals that determining the positions $\{\bar{z}_k\}$ in (42) is identical to the task of finding the n eigenvalues corresponding to the n 'main invariants' $\{n\,\bar{\mu}_l\}$ and thus equivalent to solving for the n solutions of the equation

$$\boxed{\bar{z}^n - \mathit{I}_1\bar{z}^{n-1} + \mathit{I}_2\bar{z}^{n-2} - \ldots + (-1)^n\mathit{I}_n = 0,} \tag{44}$$

where the principal invariants $\{\mathit{I}_l\}$ follow from inserting the values for the main invariants $\{n\,\bar{\mu}_l\}$ into (4), replacing J_l by $\{n\,\bar{\mu}_l\}$ and I_k by I_k. Eq. (44) represents the monic polynomial (10) whose roots provide the integration points.

Application of the chain rule of differentiation to Eq. (38) yields

$$\mathrm{EWI}\,[\psi]_{,\mathbf{C}} = \frac{1}{n}\sum_{k=1}^{n}\psi'(z_k)\,z_{k,\mathbf{C}}\,, \tag{45}$$

and

$$\mathrm{EWI}\,[\psi]_{,\mathbf{CC}} = \frac{1}{n}\sum_{k=1}^{n}\left[\psi''(z_k)\,z_{k,\mathbf{C}}\otimes z_{k,\mathbf{C}} + \psi'(z_k)\,z_{k,\mathbf{CC}}\right]\,, \tag{46}$$

and delivers the terms that specify stress and stiffness according to Eq. (1). As closed form solutions for roots of general polynomial functions of degree 5 do not exist, it seems that at least the cases $n \geq 5$ would necessitate a numeric approach. The straightforward solutions for linear, quadratic and cubic equations are discussed in Appendix B.

Remark 1 (*Complex Integration Points*)**.** Since all central moments $\{\bar{\mu}_l\}$ and thus all the principal invariants $\{\mathit{I}_l\}$ are real valued, it follows from the fundamental theorem of algebra that Eq. (44) has n complex roots and that any non-real root occurs in a complex conjugate pair (see also Supplementary Fig. 1). Notably, this property implies that the power series (40) remains real, which is a direct consequence of the following fundamental properties of complex analysis: Let $z = a + ib$ and $\hat{z} = a - ib$ its conjugate, where a and b denote the real (Re) and imaginary (Im) part of z, then

$$\mathrm{Re}\,\hat{z}^k = \mathrm{Re}\,z^k, \quad \mathrm{Im}\,\hat{z}^k = -\mathrm{Im}\,z^k, \tag{47}$$

which can be easily proven by calculation. Hence, for a complex analytic function $\psi(z) = \sum_{k=0}^{\infty} C_k z^k$, one finds

$$\psi(\hat{z}) = \hat{\psi}(z) \quad \Rightarrow \quad \psi(z) + \psi(\hat{z}) = 2\mathrm{Re}\,\psi(z), \tag{48}$$

showing that the sum of ψ evaluated at z and its conjugate $\hat{z}$ is real and equals twice $\psi(z)$.

4. Numerical determination of integration points and weights

We have shown previously in [14] that the Gauss 3-point rule already achieves remarkably high accuracy. Nevertheless, it might be desirable to increase the accuracy, particularly for highly non-linear fibre strain–energy density functions ψ. To this end, we here provide a numerical procedure to determine the n integration points for the n-point Gaussian and equal weights quadratures, respectively, as well as the corresponding weights for the former. To this end, we make use of the analogy between computing the zeros of the polynomials (35), (44), and solving the eigenvalue problem for the corresponding companion matrices as resumed in Section 2.3.

4.1. Equal weights rule

The monic polynomial (44) has the companion matrix (11) $\mathsf{M} \in \mathbb{R}^{n\times n}$

$$\mathsf{M} = \begin{bmatrix} 0 & 0 & \ldots & 0 & (-1)^{n-1}\mathit{I}_{n-0}\\ 1 & 0 & \ldots & 0 & (-1)^{n-2}\mathit{I}_{n-1}\\ 0 & 1 & \ldots & 0 & (-1)^{n-3}\mathit{I}_{n-2}\\ \vdots & \vdots & \ddots & \vdots & \vdots\\ 0 & 0 & \ldots & 1 & \mathit{I}_1 \end{bmatrix}. \tag{49}$$

Solving the eigenvalue problem for M provides the eigenvalues $\{\bar{z}_k\}$ and eigenvectors $\{\mathsf{v}_k\}$, from which V is assembled according to (13).

The derivatives of $\{\bar{z}_k\}$ with respect to $\mathbf{C}$, required to compute stress and tangent tensors (1), can be computed by use of the representation (15)

$$\mathsf{M}_{\alpha\beta} = \sum_{k=1}^{n} \bar{z}_k (\mathsf{P}_k)_{\alpha\beta}, \tag{50}$$

in terms of 'eigenprojections' P_k, where for the sake of clarity we use index notation and the Einstein summation convention, employ Latin letters running from 1 to 3 to indicate the components of tensors with respect to an orthogonal basis, and Greek letters for the components of matrices, running from 1 to n. By virtue of the chain rule of differentiation one finds

$$\bar{z}_{k,C_{ij}} = \bar{z}_{k,\mathsf{M}_{\alpha\beta}} \mathsf{M}_{\alpha\beta,C_{ij}} = (\mathsf{P}_k)_{\beta\alpha} \mathsf{M}_{\alpha\beta,C_{ij}}, \tag{51}$$

where we used the relation (16), and

$$\bar{z}_{k,C_{ij}C_{kl}} = (\mathsf{P}_k)_{\beta\alpha,\mathsf{M}_{\gamma\delta}} \mathsf{M}_{\alpha\beta,C_{ij}} \mathsf{M}_{\gamma\delta,C_{kl}} + (\mathsf{P}_k)_{\beta\alpha} \mathsf{M}_{\alpha\beta,C_{ij}C_{kl}}, \tag{52}$$

where according to Eq. (17)

$$(\mathsf{P}_k)_{\beta\alpha,\mathsf{M}_{\gamma\delta}} = \sum_{\substack{j=1 \\ j\neq k}}^{n} \frac{(\mathsf{P}_k)_{\beta\gamma}(\mathsf{P}_j)_{\delta\alpha} + (\mathsf{P}_j)_{\beta\gamma}(\mathsf{P}_k)_{\delta\alpha}}{\bar{z}_k - \bar{z}_j}. \tag{53}$$

Here M and P_k are not symmetric and hence the expressions (51) and (53) differ from their symmetric counterparts, cf. e.g. Eqs. 124,125 in Ref. [9]. Noteworthy, because only the last row of M is dependent on $\mathbf{C}$ for the numeric implementation of Eqs. (51), (52) and (53) the indices β and δ may be fixed to n. Moreover, the derivatives of M can be calculated by means of the chain rule, noting that the last row of M (49) depends on $\mathcal{I}_k$, $k = 1, 2, \dots, n$ (42), which are functions of $\bar{\mu}_j$, $j = 2, 3, \dots, n$, and hence of the invariants A and B of $\mathbf{C}$ (25), cf. Table A.1.

By definition (43), the numerical procedure to compute energy (18), stress and tangent tensors (1) is completed by insertion of the relations

$$z_k = \bar{z}_k + \mu_1, \quad z_{k,\mathbf{C}} = \bar{z}_{k,\mathbf{C}} + \mu_{1,\mathbf{C}}, \quad z_{k,\mathbf{CC}} = \bar{z}_{k,\mathbf{CC}}, \tag{54}$$

into the EWI Eqs. (38), (45) and (46).

4.2. Gauss rule

Brought into the representation (35) one identifies the companion matrix (11) $\mathsf{M} \in \mathbb{R}^{n\times n}$ of the orthogonal polynomial Q_n/c_n as

$$\mathsf{M} = \begin{bmatrix} 0 & 0 & \dots & 0 & -c_0/c_n \\ 1 & 0 & \dots & 0 & -c_1/c_n \\ 0 & 1 & \dots & 0 & -c_2/c_n \\ \vdots & \vdots & \ddots & \vdots & \vdots \\ 0 & 0 & \dots & 1 & -c_{n-1}/c_n \end{bmatrix}. \tag{55}$$

The task of identifying the integration points x_k as well as their derivatives $x_{k,\mathbf{C}}$ and $x_{k,\mathbf{CC}}$ is analogous to the procedure in Section 4.1 for z_k and its derivatives, i.e. Eqs. (50)–(53). However, since all Gauss integration points x_k are real-valued, only operations with real numbers are involved. Analogous to Eq. (54) one obtains in view of (31)

$$x_k = \bar{x}_k + \mu_1, \quad x_{k,\mathbf{C}} = \bar{x}_{k,\mathbf{C}} + \mu_{1,\mathbf{C}}, \quad x_{k,\mathbf{CC}} = \bar{x}_{k,\mathbf{CC}}, \tag{56}$$

which need to be inserted in the GI equations (30), (36) and (37). Again, the derivatives of M in Eqs. (51) and (52) required to compute $x_{k,\mathbf{C}}$ and $x_{k,\mathbf{CC}}$ follow from the chain rule, since the last row of M (55) depends on c_k, $k = 0, 1, \dots, n$ (34), which are functions of $\bar{\mu}_j$, $j = 2, 3, \dots, n$, and hence of the invariants A and B of $\mathbf{C}$ (25), cf. Table A.1.

In addition to integration points, the GI rule requires the determination of the integration weights w_k and their derivatives $w_{k,\mathbf{C}}, w_{k,\mathbf{CC}}$ with respect to $\mathbf{C}$. To this end, we use the following property

$$\underbrace{\begin{bmatrix} \bar{x}_1^0 & \bar{x}_2^0 & \dots & \bar{x}_n^0 \\ \bar{x}_1 & \bar{x}_2 & \dots & \bar{x}_n \\ \vdots & \vdots & \ddots & \vdots \\ \bar{x}_1^{n-1} & \bar{x}_2^{n-1} & \dots & \bar{x}_n^{n-1} \end{bmatrix}}_{\mathsf{W}} \underbrace{\begin{bmatrix} \bar{w}_1 \\ \bar{w}_2 \\ \vdots \\ \bar{w}_n \end{bmatrix}}_{\mathsf{w}} = \underbrace{\begin{bmatrix} \bar{\mu}_1 \\ \bar{\mu}_2 \\ \vdots \\ \bar{\mu}_n \end{bmatrix}}_{\bar{\mathsf{m}}}, \tag{57}$$

which allows computing the weights w as solution to this linear system of equations, i.e.

$$\mathsf{w} = \mathsf{W}^{-1} \bar{\mathsf{m}}. \tag{58}$$

For the first derivatives $w_{k,\mathbf{C}} = w_{k,C_{ij}} \boldsymbol{e}_i \otimes \boldsymbol{e}_j$, from Eq. (57) one derives

$$\mathsf{w}_{,C_{ij}} = \mathsf{W}^{-1} \left(\bar{\mathsf{m}}_{,C_{ij}} - \mathsf{W}_{,C_{ij}} \mathsf{w} \right), \tag{59}$$

where

$$\mathsf{W}_{,C_{ij}} \mathsf{w} = \underbrace{\begin{bmatrix} 0 & & & & \\ & 1 & & & \\ & & 2 & & \\ & & & \ddots & \\ & & & & n-1 \end{bmatrix}}_{\mathsf{D}} \underbrace{\begin{bmatrix} 0 & 0 & \dots & 0 \\ \bar{x}_1^0 & \bar{x}_2^0 & \dots & \bar{x}_n^0 \\ \bar{x}_1^1 & \bar{x}_2^1 & \dots & \bar{x}_n^1 \\ \vdots & \vdots & \ddots & \vdots \\ \bar{x}_1^{n-2} & \bar{x}_2^{n-2} & \dots & \bar{x}_n^{n-2} \end{bmatrix}}_{\mathsf{X}} \begin{bmatrix} w_1 \bar{x}_{1,C_{ij}} \\ w_2 \bar{x}_{2,C_{ij}} \\ w_3 \bar{x}_{3,C_{ij}} \\ \vdots \\ w_n \bar{x}_{n,C_{ij}} \end{bmatrix}, \tag{60}$$

and the rows of W can be found again in X. For the second derivatives $w_{k,\mathbf{CC}} = w_{k,C_{ij}C_{kl}} \boldsymbol{e}_i \otimes \boldsymbol{e}_j \otimes \boldsymbol{e}_k \otimes \boldsymbol{e}_k$, we further derive

$$\mathsf{w}_{,C_{ij}C_{kl}} = \mathsf{W}^{-1} \left(\bar{\mathsf{m}}_{,C_{ij}C_{kl}} - \mathsf{W}_{,C_{ij}C_{kl}} \mathsf{w} - \mathsf{W}_{,C_{ij}} \mathsf{w}_{,C_{kl}} - \mathsf{W}_{,C_{kl}} \mathsf{w}_{,C_{ij}} \right), \tag{61}$$

where the last two terms, in analogy to Eq. (60), can be computed from

$$\mathsf{W}_{,C_{ij}} \mathsf{w}_{,C_{kl}} = \mathsf{D}\mathsf{X} \begin{bmatrix} w_{1,C_{kl}} \bar{x}_{1,C_{ij}} \\ w_{2,C_{kl}} \bar{x}_{2,C_{ij}} \\ \vdots \\ w_{n,C_{kl}} \bar{x}_{n,C_{ij}} \end{bmatrix}, \tag{62}$$

and

$$\mathsf{W}_{,C_{ij}C_{kl}} \mathsf{w} = \mathsf{D}\mathsf{X} \begin{bmatrix} w_1 \bar{x}_{1,C_{ij}C_{kl}} \\ w_2 \bar{x}_{2,C_{ij}C_{kl}} \\ w_3 \bar{x}_{3,C_{ij}C_{kl}} \\ \vdots \\ w_n \bar{x}_{n,C_{ij}C_{kl}} \end{bmatrix} + \mathsf{D} \underbrace{\begin{bmatrix} 0 & 0 & \dots & 0 \\ 0 & 0 & \dots & 0 \\ \bar{x}_1^0 & \bar{x}_2^0 & \dots & \bar{x}_n^0 \\ \vdots & \vdots & \ddots & \vdots \\ \bar{x}_1^{n-2} & \bar{x}_2^{n-2} & \dots & \bar{x}_n^{n-2} \end{bmatrix}}_{\mathsf{Y}} \begin{bmatrix} w_1 \bar{x}_{1,C_{ij}} \bar{x}_{1,C_{kl}} \\ w_2 \bar{x}_{2,C_{ij}} \bar{x}_{2,C_{kl}} \\ w_3 \bar{x}_{3,C_{ij}} \bar{x}_{3,C_{kl}} \\ \vdots \\ w_n \bar{x}_{n,C_{ij}} \bar{x}_{n,C_{kl}} \end{bmatrix}, \tag{63}$$

and the rows of X (and thus W) can be found again in Y.

5. Application to the full-network model of rubber-elasticity

The here elaborated numerical procedures to apply the n-point GI and EWI method, as well as the EWI method with 3 points (Appendix B) are illustrated in application to the non-Gaussian affine full network model for rubber elasticity. To this end, a 'fibre' is associated with the end-to-end vector $\boldsymbol{r}$ of a long-chain molecule, that changes its squared length from r_0^2 in the reference state of the chain network to $r^2 = \Lambda r_0^2$ in the current configuration. As usual, r_0^2 is set to the mean squared end-to-end distance of an unconstrained chain, so that it can be expressed in terms the number N and length l of the links of the chain as $r_0^2 = Nl^2$ [see e.g. 29]. Different variants of the non-Gaussian chain model will be considered and the free energy of the entropy-elastic single chains $\psi(\Lambda)$ is expressed in terms of the affine square stretch Λ, respectively. Accordingly the network free energy (18) is given by

$$\Psi = \nu \left(\mathrm{E}\left[\psi(\Lambda)\right] - \mathrm{E}\left[\psi(1)\right] \right) = \Psi_r - \Psi_{r_0}, \tag{64}$$

where $\Psi_{r_0} = \nu \mathrm{E}\left[\psi(1)\right] = C$ is constant.

5.1. Summary of EWI, GI and benchmarks

The new concepts are compared to two existing approaches as benchmarks: Spherical cubature with a very large number of integration points is used to establish a numerical ground truth, and analytical integration on the sphere based on a Taylor expansion of the integrand is employed as a potential alternative. All methods are briefly resumed in what follows. They were implemented in Python 3.8, using the NumPy module v1.19.2.

5.1.1. n-Point equal weights quadrature

The general concept of the equal weights integration rule and its differentiation has been introduced in Section 3.2 of the present work. In Section 4.1 we elaborated in detail how to determine the integration points and their derivatives in case of n-point rule. Algorithm 1 summarises the computational steps.

5.1.2. n-Point Gauss quadrature

The Gauss type quadrature rule recently introduced for anisotropic fibrous materials [14], has been summarised in Section 3.1. While the previous work had focused on the 3-point rule, we have elaborated the n-point version in Section 4.2 of this work. The computational steps are summarised in Algorithm 2.

function EWI (n, $\mathbf{F}$, ψ, ψ', ψ'')
  compute μ_1 and $\bar{\mu}_2$ (Section 2.5)
  if $\bar{\mu}_2 <$ **tol then**
    $\Psi = \psi(\mu_1)$
    $\Psi_{,\mathbf{C}} = \psi'(\mu_1)\,\mathbf{I}$
    $\Psi_{,\mathbf{CC}} = \psi''(\mu_1)\,\mathbb{H}_2\,, \quad \mathbb{H}_2 = (\mathbf{I}\otimes\mathbf{I} + 2\,\mathbf{I}\boxtimes\mathbf{I})/15$
  else
    compute $\{I_k\}$ (44), $\{I_{k,\mathbf{C}}\}$ and $\{I_{k,\mathbf{CC}}\}$
    compute M (49), $\mathsf{M}_{\alpha\beta,C_{ij}}$, $\mathsf{M}_{\alpha\beta,C_{ij}C_{kl}}$
    diagonalise M and obtain V, V^{-1} and $\{\bar{z}_k\}$ (12)
    compute $\{\mathsf{P}_k\}$ (15) and $\{(\mathsf{P}_k)_{\beta\alpha,M_{\gamma\delta}}\}$ (17), (53)
    compute $\{z_{k,\mathbf{C}}\}$ and $\{z_{k,\mathbf{CC}}\}$ (51), (52), (54)
    $\Psi = \mathrm{EWI}\,[\psi]$
    $\Psi_{,\mathbf{C}} = \mathrm{EWI}\,[\psi]_{,\mathbf{C}}$ (45)
    $\Psi_{,\mathbf{CC}} = \mathrm{EWI}\,[\psi]_{,\mathbf{CC}}$ (46)
  end
  $\mathbf{S} = 2\,\Psi_{,\mathbf{C}}$
  $\sigma_{ij} = 2J^{-1}F_{iI}F_{jJ}(\Psi_{,\mathbf{C}})_{IJ}$
  $\mathbb{C} = 4\Psi_{,\mathbf{CC}}$
return Ψ, σ_{ij}, $\mathbb{C}$

Algorithm 1: EWI: Pseudo-code for n-point rule. For the sake of simplicity in writing we set $\Psi = \mathrm{E}\,[\psi]$ in this example, i.e. neglect ν and Ψ_{r_0} in Eq. (64).

function GI (n, $\mathbf{F}$, ψ, ψ', ψ'')
  compute μ_1 and $\bar{\mu}_2$ (Section 2.5)
  if $\bar{\mu}_2 <$ **tol then**
    $\Psi = \psi(\mu_1)$
    $\Psi_{,\mathbf{C}} = \psi'(\mu_1)\,\mathbf{I}$
    $\Psi_{,\mathbf{CC}} = \psi''(\mu_1)\,\mathbb{H}_2\,, \quad \mathbb{H}_2 = (\mathbf{I}\otimes\mathbf{I} + 2\,\mathbf{I}\boxtimes\mathbf{I})/15$
  else
    compute $\{c_k\}$ (34), $\{c_{k,\mathbf{C}}\}$ and $\{c_{k,\mathbf{CC}}\}$
    compute M (55), $\mathsf{M}_{\alpha\beta,C_{ij}}$, $\mathsf{M}_{\alpha\beta,C_{ij}C_{kl}}$
    diagonalise M and obtain V, V^{-1} and $\{\bar{x}_k\}$ (12)
    compute $\{\mathsf{P}_k\}$ (15) and $\{(\mathsf{P}_k)_{\beta\alpha,M_{\gamma\delta}}\}$ (17)
    compute $\{x_{k,\mathbf{C}}\}$ and $\{x_{k,\mathbf{CC}}\}$ (56)
    compute $\bar{\mathsf{m}}$, $\bar{\mathsf{m}}_{,C_{ij}}$, $\bar{\mathsf{m}}_{,C_{ij}C_{kl}}$, W, W^{-1} (57), (58)
    assemble X (59) and Y (61) from W
    determine $\{w_k\}$ from w (57)
    compute $\mathsf{W}_{,C_{ij}}\mathsf{w}$ (60)
    determine $\{w_{k,C_{ij}}\}$ from $\mathsf{w}_{,C_{ij}}$ (59)
    compute $\mathsf{W}_{,C_{ij}}\mathsf{w}_{,C_{kl}}$, $\mathsf{W}_{,C_{kl}}\mathsf{w}_{,C_{ij}}$ (62) and $\mathsf{W}_{,C_{ij}C_{kl}}\mathsf{w}$ (63)
    determine $\{w_{k,C_{ij}C_{kl}}\}$ from $\mathsf{w}_{,C_{ij}C_{kl}}$ (61)
    $\Psi = \mathrm{GI}\,[\psi]$
    $\Psi_{,\mathbf{C}} = \mathrm{GI}\,[\psi]_{,\mathbf{C}}$ (36)
    $\Psi_{,\mathbf{CC}} = \mathrm{GI}\,[\psi]_{,\mathbf{CC}}$ (37)
  end
  $\mathbf{S} = 2\,\Psi_{,\mathbf{C}}$
  $\sigma_{ij} = 2J^{-1}F_{iI}F_{jJ}(\Psi_{,\mathbf{C}})_{IJ}$
  $\mathbb{C} = 4\Psi_{,\mathbf{CC}}$
return Ψ, σ_{ij}, $\mathbb{C}$

Algorithm 2: GI: Pseudo-code for n-point rule. For the sake of simplicity in writing we set $\Psi = \mathrm{E}\,[\psi]$ in this example, i.e. neglect ν and Ψ_{r_0} in Eq. (64).

5.1.3. Spherical cubature

Using spherical cubature (19) to approximate the averaged chain free energy, the related network free energy Ψ_r (18) can be defined as [cf. e.g. 23,39,40]

$$\Psi_r = \nu\,\mathrm{E}[\psi] \approx \nu\,\mathrm{SC}[\psi] = \nu \sum_{k=1}^{n} \psi(\mathbf{C} : \boldsymbol{N}_k \otimes \boldsymbol{N}_k)\, w_k \tag{65}$$

with pairs of integration points and weights $\{\boldsymbol{N}_k, w_k\}$.

As a consequence the stress and elasticity tensors for an unconstrained material (1) follow as

$$\mathbf{S} \approx 2\nu\,\mathrm{SC}[\psi]_{,\mathbf{C}} = 2\nu \sum_{k=1}^{n} \psi'(\mathbf{C} : \boldsymbol{N}_k \otimes \boldsymbol{N}_k)\, \boldsymbol{N}_k \otimes \boldsymbol{N}_k\, w_k \tag{66}$$

and

$$\mathbb{C} \approx 4\nu\,\mathrm{SC}[\psi]_{,\mathbf{CC}} = 4\nu \sum_{k=1}^{n} \psi''(\mathbf{C} : \boldsymbol{N}_k \otimes \boldsymbol{N}_k)\, \boldsymbol{N}_k \otimes \boldsymbol{N}_k \otimes \boldsymbol{N}_k \otimes \boldsymbol{N}_k\, w_k. \tag{67}$$

In this paper, spherical cubature will be used to define a numerical ground truth for the macroscopic energy Ψ and the associated stress measures (1). Therefore we selected a highly accurate Lebedev scheme, i.e. SC 5810-131, which with $n = 5810$ points exactly integrates spherical polynomials (in x, y, z) up to order 131 [41,42].

5.1.4. Taylor expansion of the integrand

Itskov et al. [27] proposed to expand the chain free energy into a (truncated) Taylor series, which leads to a moment series, viz.

$$\Psi = \nu\,\mathrm{E}[\psi] \approx \nu\,\mathrm{TE}[\psi] = \nu\,\mathrm{E}\left[\sum_{k=0}^{n} \frac{1}{k!} \frac{\partial^k \psi}{\partial \Lambda^k}(\Lambda^*)(\Lambda - \Lambda^*)^k\right] = \nu \sum_{k=0}^{n} \frac{1}{k!} \frac{\partial^k \psi}{\partial \Lambda^k}(\Lambda^*)\, \mu_k^*, \tag{68}$$

where $\mu_k^* = \mathrm{E}\left[(\Lambda - \Lambda^*)^k\right]$ are the moments of the square stretch distribution with respect to Λ^*. In particular for $\Lambda^* = \mu_1$ these moments become the central moments, i.e. $\mu_k^* = \bar{\mu}_k = \mathrm{E}[\Lambda]$, for which we provided the first 30 in Appendix A (Table A.1), and a closed form derivation to obtain terms up to arbitrary n can be found in [9]. For other choices of Λ^* the moments can be related to the central moments with help of the binomial formula as [cf. e.g. 27]

$$\mu_k^* = \mathrm{E}\left[(\Lambda - \mu_1 + \mu_1 - \Lambda^*)^k\right] = \mathrm{E}\left[\sum_{i+j=k} \binom{k}{i,j} (\Lambda - \mu_1)^i (\mu_1 - \Lambda^*)^j\right] = \sum_{i+j=k} \binom{k}{i,j} \bar{\mu}_i\, (\mu_1 - \Lambda^*)^j. \tag{69}$$

The stress and tangent tensors for an unconstrained material (1) can be deduced as

$$\mathbf{S} \approx 2\nu\,\mathrm{TE}[\psi]_{,\mathbf{C}} = 2\nu \sum_{k=0}^{n} \left[\psi'(\Lambda^*)\mu_k^*\, \Lambda^*{}_{,\mathbf{C}} + \psi(\Lambda^*)\, \mu_{k,\mathbf{C}}^*\right] \tag{70}$$

and

$$\mathbb{C} \approx 4\nu\,\mathrm{TE}[\psi]_{,\mathbf{CC}} = 4\nu \sum_{k=0}^{n} \left[\, \psi''(\Lambda^*)\mu_k^*\, \Lambda^*{}_{,\mathbf{C}} \otimes \Lambda^*{}_{,\mathbf{C}} + \psi'(\Lambda^*)\, \Lambda^*{}_{,\mathbf{C}} \otimes^{\mathrm{s}} \mu_{k,\mathbf{C}}^* \;+\; \psi'(\Lambda^*)\mu_k^*\, \Lambda^*{}_{,\mathbf{CC}} + \psi(\Lambda^*)\, \mu_{k,\mathbf{CC}}^* \,\right], \tag{71}$$

where the abbreviation $\mathbf{A} \otimes^{\mathrm{s}} \mathbf{B} = \mathbf{A} \otimes \mathbf{B} + \mathbf{B} \otimes \mathbf{A}$ was used. For the special case $\Lambda^* = \mu_1$ one has $\Lambda^*{}_{,\mathbf{C}} = \mathbf{I}/3$ and $\Lambda^*{}_{,\mathbf{CC}} = \mathbb{O}$ as well as $\mu_{k,\mathbf{C}}^* = \bar{\mu}_{k,\mathbf{C}}$ and $\mu_{k,\mathbf{CC}}^* = \bar{\mu}_{k,\mathbf{CC}}$. Other choices of Λ^* require an individual approach to determine $\Lambda^*{}_{,\mathbf{C}}$ and $\Lambda^*{}_{,\mathbf{CC}}$. For example, following Itskov et al. [27], we will also use $\Lambda^* = \Lambda_1/2$, i.e. half the squared first principal stretch, in the present work. In this case

$$\Lambda^*{}_{,\mathbf{C}} = \frac{\mathbf{P}_1}{2}, \quad \Lambda^*{}_{,\mathbf{CC}} = \frac{\mathbf{P}_{1,\mathbf{C}}}{2}. \tag{72}$$

In any case, once $\Lambda^*{}_{,\mathbf{C}}$ and $\Lambda^*{}_{,\mathbf{CC}}$ are defined, the derivatives of the corresponding moments μ^* can be obtained from Eq. (69) as

$$\mu_{k,\mathbf{C}}^* = \sum_{i+j=k} \binom{k}{i,j} \left[(\mu_1 - \Lambda^*)^j\, \bar{\mu}_{i,\mathbf{C}} + \bar{\mu}_i\, j(\mu_1 - \Lambda^*)^{j-1} \left(\frac{\mathbf{I}}{3} - \Lambda^*{}_{,\mathbf{C}}\right)\right] \tag{73}$$

and

$$\begin{aligned} \mu_{k,\mathbf{CC}}^* = \sum_{i+j=k} \binom{k}{i,j} \Bigg[& j(\mu_1 - \Lambda^*)^{j-1}\, \bar{\mu}_{i,\mathbf{C}} \otimes^{\mathrm{s}} \left(\frac{\mathbf{I}}{3} - \Lambda^*{}_{,\mathbf{C}}\right) + (\mu_1 - \Lambda^*)^j\, \bar{\mu}_{i,\mathbf{CC}} \\ & + \bar{\mu}_i\, j(j-1)(\mu_1 - \Lambda^*)^{j-2} \left(\frac{\mathbf{I}}{3} - \Lambda^*{}_{,\mathbf{C}}\right)^{\otimes 2} \;-\; \bar{\mu}_i\, j(\mu_1 - \Lambda^*)^{j-1}\, \Lambda^*{}_{,\mathbf{CC}} \Bigg]. \end{aligned} \tag{74}$$

5.2. Entropy elastic models of non-Gaussian chains

The integration methods are compared for four different variants of the entropy-elastic model that provides the relation between the end-to-end stretch λ of a non-Gaussian long chain molecule and the force f at its ends.

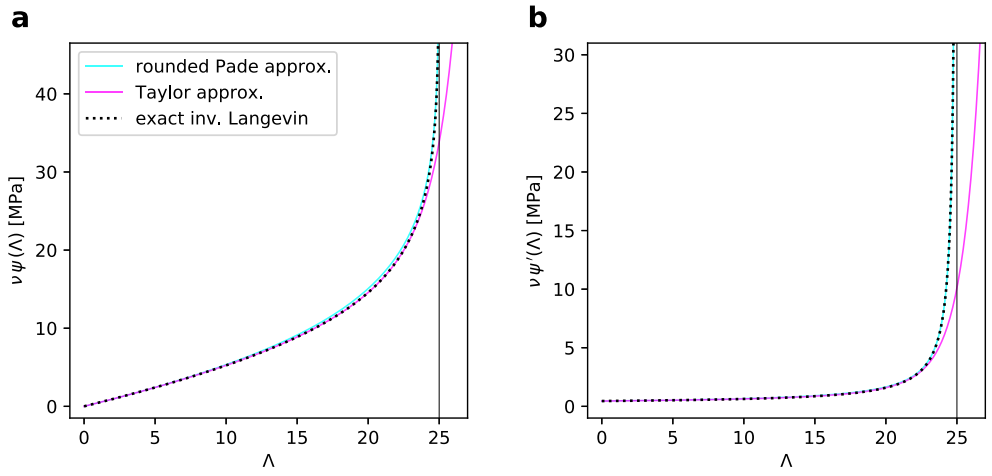

Fig. 1. Rounded Padé [31] and Taylor-series approximations of the inverse Langevin model: Chain free energy (a) and its derivative (b) with respect to Λ, based on Eqs. (78) and (80). The 'exact' result in (b) was computed based on Eq. (75), using $f(\lambda) = \psi'(\lambda^2)\,2\lambda$, i.e. $\psi'(\lambda(f)^2) = 1/(2\,\lambda(f))f$, and subsequently plotting its integral $\psi = \int \psi' d\lambda$ as a function of f and $\lambda(f)$ in (a).

5.2.1. Rounded Padé-approximation of inverse Langevin function

The most common model to represent the relation between the end-to-end stretch λ of a non-Gaussian long chain molecule and force f at its ends is due to Kuhn and Grün [43] and can be expressed as [cp. 29, Eq. 6.10]

$$f(\lambda) = \frac{k_B \Theta}{l}\,\mathscr{L}^{-1}\left(\frac{\lambda}{\sqrt{N}}\right), \tag{75}$$

where Θ stands for the absolute temperature, k_B is Boltzmann's constant, and $\mathscr{L}^{-1}(\cdot)$ denotes the inverse of the Langevin function

$$\mathscr{L}(x) = \coth(x) + \frac{1}{x}. \tag{76}$$

Since there is no exact closed form expression for the inverse $\mathscr{L}^{-1}(x)$ of $\mathscr{L}(x)$, different approximations of this inverse have been used.

As a first example we will use the rounded Padé-approximation by Cohen [31]

$$\mathscr{L}^{-1}(x) \approx x\,\frac{3 - x^2}{1 - x^2}. \tag{77}$$

Inserting this approximation into Eq. (75), the free energy $\psi(\Lambda)$ (per initial end-to-end length) of the chain follows by the integration [cf. 27, Eq. 25]

$$\psi(\Lambda) := \int_0^{\sqrt{\Lambda}} f_{\text{Pade}}(\lambda)\,\mathrm{d}\lambda = \frac{k_B \Theta}{l}\sqrt{N}\left(\frac{1}{2}\frac{\Lambda}{N} - \ln\left(1 - \frac{\Lambda}{N}\right)\right), \tag{78}$$

where $\Lambda = \lambda^2$ is the square stretch. The total free energy of the chain is obtained by multiplication with the initial end-to-end length $r_0 = \sqrt{N}\,l$. The model is illustrated in Fig. 1.

5.2.2. Taylor approximation of inverse Langevin function

Another classical method to approximate the non-Gaussian chain behaviour is a Taylor series expansion [cf. 29]. We here compare with the Taylor series expression for the inverse Langevin function of order 59 [44]

$$\mathscr{L}^{-1}(x) \approx \sum_{k=0}^{59} C_k x^k = \sum_{k=0}^{29} C_{2k+1} x^{2k+1}, \tag{79}$$

and we refer to Tab. 2 in Itskov et al. [44] for the non-zero Taylor coefficients C_{2k+1}. Inserting this approximation into Eq. (75), the corresponding (end-to-end length specific) free energy follows as [cp. 27, Eq. 18]

$$\psi(\Lambda) := \int_0^{\sqrt{\Lambda}} f_{\text{Taylor}}(\lambda)\,\mathrm{d}\lambda = \frac{k_B \Theta}{l}\sqrt{N}\sum_{k=0}^{29} C_{2k+1}\,\frac{1}{2k+2}\left(\frac{\Lambda}{N}\right)^{k+1}, \tag{80}$$

illustrated in Fig. 1, and we note that this expression is analytic on $\mathbb{C}$.

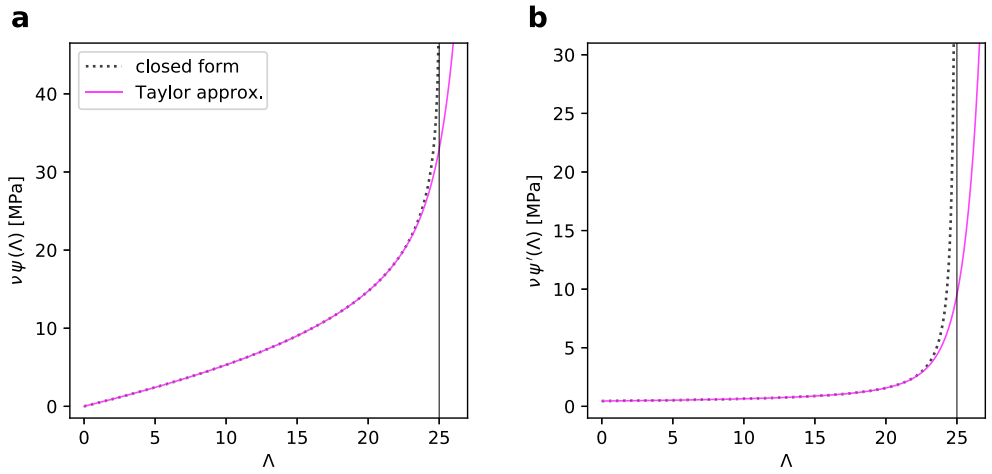

Fig. 2. Closed-form solution and Taylor-series approximation of Ilg model [32]: Chain free energy (a) and its derivative (b) with respect to Λ, based on Eqs. (82) and (83).

5.2.3. Closed form representation of model by Ilg et al. [32]

Another model for the non-Gaussian theory of rubber elasticity was proposed by Ilg et al. [32] and has been used in [45,46]. In this model the force f in a polymer chain is related to its end-to-end stretch λ as [32]

$$f(\lambda) = \frac{9}{\pi^2}\frac{k_\mathrm{B}\Theta}{l}\left(\frac{\sqrt{N}}{\lambda} - \pi\cot\left(\pi\frac{\lambda}{\sqrt{N}}\right)\right), \tag{81}$$

which is associated to the chain free energy [cf. 45–47]

$$\psi(\Lambda) = \int_0^{\sqrt{\Lambda}} f(\lambda)\,\mathrm{d}\lambda = \frac{9}{\pi^2}\frac{k_\mathrm{B}\Theta}{l}\sqrt{N}\,\ln\left(\frac{\pi\sqrt{\frac{\Lambda}{N}}}{\sin\left(\pi\sqrt{\frac{\Lambda}{N}}\right)}\right), \tag{82}$$

and $\Lambda = \lambda^2$ is the squared stretch.

5.2.4. Taylor approximation of model by Ilg et al. [32]

Since EWI for $n > 3$ requires ψ to be complex analytic, a truncated Taylor series of the model (81) was considered in addition to the closed form expression (82). Given the expansion $\ln(x/\sin(x)) = \sum_{k=1}^{\infty} C_k x^{2k}$, the substitution $x^2 = \pi^2\Lambda/N$ and consideration of terms up to $k = 34$ leads to

$$\psi(\Lambda) = \frac{9}{\pi^2}\frac{k_\mathrm{B}\Theta}{l}\sqrt{N}\sum_{k=1}^{34} C_k\pi^{2k}\left(\frac{\Lambda}{N}\right)^k \tag{83}$$

with coefficients C_k provided in Appendix C (Table C.2). Both the exact model (82) and its approximation (83) are illustrated in Fig. 2.

5.3. Material properties

With ν (dimension per area) reflecting the chain 'density' (total chain end-to-end initial length per referential network volume), Eq. (18) provides the network strain–energy density Ψ. In order to compare the results with those obtained for the Taylor-series based model in Itskov et al. [27], we choose the material parameters corresponding to an example therein, and set $n = 25$ and $\nu\,k_\mathrm{B}\Theta/(l\sqrt{N}) =: C_R = 0.3\,\mathrm{MPa}$. In addition, we assumed that the resulting rubber-like material was hyperelastic, isotropic and incompressible. Due to the latter property, the stress and elasticity tensors contain additional contributions related to the kinematic constraint [see e.g. 48]. For the 2nd Piola–Kirchhoff stress in particular, we modify Eq. (1), so that

$$\mathbf{S} = 2\frac{\partial\hat{\Psi}}{\partial\mathbf{C}} - p\,\mathbf{C}^{-1}, \tag{84}$$

where p is the hydrostatic pressure determined from the stress boundary conditions.

5.4. Load cases

The load cases of uniaxial tension and equibiaxial tension were studied and the non-Gaussian chain free energy ψ for each of the entropic chain models provided in Section 5.2 was integrated by means of the methods presented in Section 5.1, respectively. Due to the isotropy of the material, we note that the corresponding kinematic states are characterised by uniaxial and equibiaxial extension with corresponding contraction in the unconstrained directions, respectively. These states are of particular interest to test the quadrature rules. When introducing a normalised representation of square stretch (Supplementary Information, Sec. 1) such that the mid-eigenvalue of $\mathbf{C}$, Λ_2, is normalised to $\Lambda_2^{\mathrm{n}} = (\Lambda_2 - \Lambda_3)/(\Lambda_1 - \Lambda_3)$, it is observed that these states represent the limit cases of $\Lambda_2^{\mathrm{n}} = 0$ and $\Lambda_2^{\mathrm{n}} = 1$ (cf. Supp. Figs. 1 and 2). Specifically, due to the assumed isotropy and incompressibility, the deformation gradient corresponding to uniaxial tension is described by

$$\mathbf{F}_{\mathrm{UA}} = \lambda_x \boldsymbol{e}_1 \otimes \boldsymbol{e}_1 + \lambda_x^{-1/2} \boldsymbol{e}_2 \otimes \boldsymbol{e}_2 + \lambda_x^{-1/2} \boldsymbol{e}_3 \otimes \boldsymbol{e}_3 \tag{85}$$

varying $\lambda_x \in [1, \sqrt{N})$. The corresponding 1st Piola–Kirchhoff stress reads

$$\mathbf{P}_{\mathrm{UA}} = P_{11} \boldsymbol{e}_1 \otimes \boldsymbol{e}_1, \tag{86}$$

since in y- and z-direction $P_{22} = P_{33} = 0$. Similarly, the deformation gradient corresponding to equibiaxial tension is described by

$$\mathbf{F}_{\mathrm{EB}} = \lambda_{xy} \boldsymbol{e}_1 \otimes \boldsymbol{e}_1 + \lambda_{xy} \boldsymbol{e}_2 \otimes \boldsymbol{e}_2 + \lambda_{xy}^{-2} \boldsymbol{e}_3 \otimes \boldsymbol{e}_3 \tag{87}$$

and varying $\lambda_{xy} \in [1, \sqrt{N})$. The 1st Piola–Kirchhoff tensor is

$$\mathbf{P}_{\mathrm{EB}} = P_{11} \boldsymbol{e}_1 \otimes \boldsymbol{e}_1 + P_{22} \boldsymbol{e}_2 \otimes \boldsymbol{e}_2, \tag{88}$$

where $P_{11} = P_{22}$, and since in z-direction one has $P_{33} = 0$.

For each state of deformation $\mathbf{F}_{\mathrm{UA}}$ as well as $\mathbf{F}_{\mathrm{EB}}$ for a series of λ_x, respectively λ_{xy}, between 1 and 5 the work-related part of the second Piola–Kirchhoff tensor $\mathbf{S}$ is computed with the integration methods in Section 5.1. Specifically, the work-related constitutive part $\mathbf{S}_{\mathrm{c}}$ of $\mathbf{S}$ is given by

$$\mathbf{S}_{\mathrm{c}} = 2\frac{\partial \Psi}{\partial \mathbf{C}} = 2\nu\, \mathrm{E}[\psi]_{,\mathbf{C}}\,, \tag{89}$$

where $\mathrm{E}[\psi]_{,\mathbf{C}}$ is to be replaced with $\mathrm{GI}[\psi]_{,\mathbf{C}}$ for the GI method $\mathrm{EWI}[\psi]_{,\mathbf{C}}$ for the EWI method $\mathrm{SC}[\psi]_{,\mathbf{C}}$ for the spherical cubature and finally $\mathrm{TE}[\psi]_{,\mathbf{C}}$ for the method using a Taylor expansion of the integrand. Notably, the EWI methods, due to the complex numbers involved, requires the chain strain–energy function to be analytic in $\mathbb{C}$. Consequently the EWI method is only applied to the Taylor approximations (80) and (83) while the other methods are also applied to the rounded Padé approximation (78) and the closed form model by Ilg et al. [32] (82). Finally, in view of the boundary conditions, the first Piola–Kirchhoff stress tensor for the special cases (86) and (88) is deduced as

$$\mathbf{P}_* = \mathbf{F}_* \mathbf{S}_{\mathrm{c}} - \underbrace{(\mathbf{F}_* \mathbf{S}_{\mathrm{c}} \mathbf{F}_*^{\mathrm{T}} : \boldsymbol{e}_3 \otimes \boldsymbol{e}_3)}_{p} \mathbf{F}_*^{-\mathrm{T}}, \tag{90}$$

where the subscript $*$ may be replaced by UA and EB.

6. Results and discussion

The proposed quadratures and benchmark methods were applied to evaluate the response of the non-Gaussian full network model under uniaxial and biaxial loads, obtained with one of the different representations of the entropy elastic chain behaviour as described in Section 5.

6.1. Response in simple and equibiaxial tension

Figs. 3 and 4 show the first Piola–Kirchhoff stress P_{11} in uniaxial and equibiaxial tension of the inverse Langevin model, using either the rounded Padé approximation (78) or the Taylor-series approximation (80), respectively. We remind that both the TE and EWI method rely on the Taylor series of the integrand, while GI can be applied to the function itself. TE and EWI hence strictly lead to the network free energy of chains whose free energy is a polynomial. Figs. 5 and 6 illustrate the corresponding results for the closed form (82) and the Taylor approximation (83) of the model by Ilg et al. [32].

The results presented in Figs. 3 and 5, and the first rows of Figs. 4 and 6, illustrate that GI represents an accurate method for computing the network response based on very few function evaluations, i.e. 3 or 4 in the shown GI 3-5 or GI 4-7 schemes, respectively, even for rational function's as Cohen's rounded Padé approximant to the inverse Langevin function. The results of the EWI method applied to the complex analytic Taylor series approximations of the inverse Langevin function and Ilg model, respectively, are shown in the second rows of Figs. 4 and 6 and are less accurate. Specifically in the equibiaxial case (d panels of Figs. 4 and 6) the shown odd EWI methods (EWI 3, 5 and 7) start deviating from the ground truth close to the extension limit $\Lambda = 5$, leading to a drastic underestimation of the ground truth, while the even ones (EWI 4,6 and 8) overestimate it. This behaviour can be explained through the positions of the integration points (Supp. Figs. 1 and 2): For equibiaxial extension, i.e. $\Lambda_1 = \Lambda_2$ and

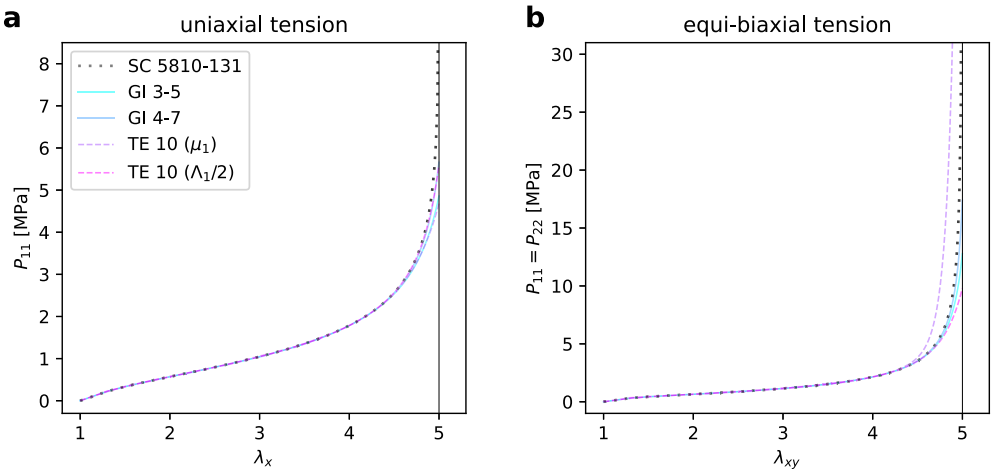

Fig. 3. Full network based on rounded Padé approximation. Non-zero components of first Piola–Kirchhoff stress in case of uniaxial (a) and equibiaxial tension (b) (cf. Section 5.4). SC 5810-131: spherical integration ground truth, GI-X-Y: Gauss integration of order Y with X points, TE: Taylor series expansion (with expansion points), cf. Section 5.1.

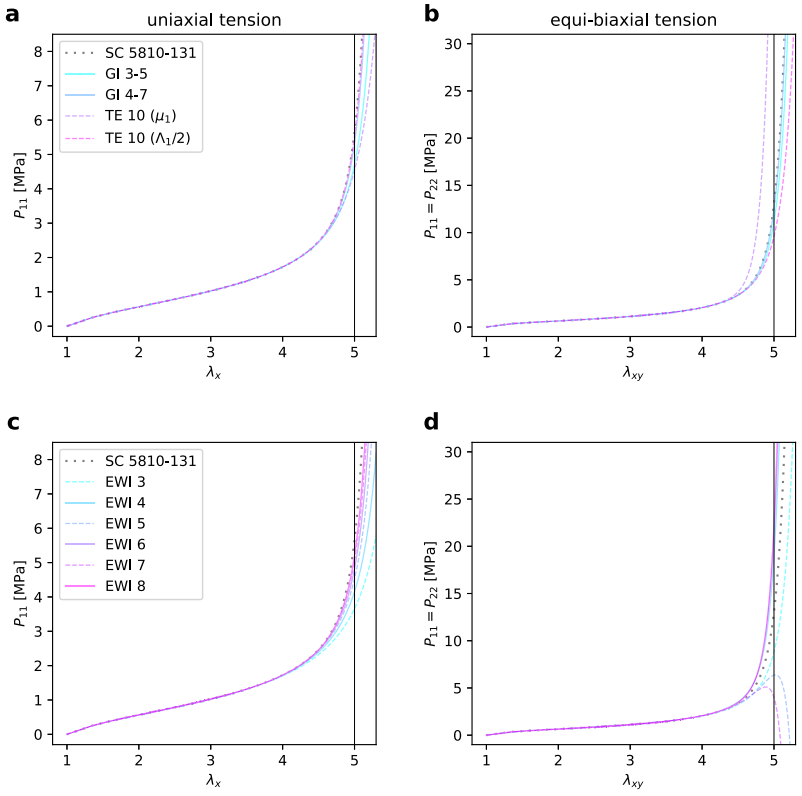

Fig. 4. Full network based on Taylor approximation of inverse Langevin model. Non-zero components of first Piola–Kirchhoff stress in case of uniaxial (a,c) and equibiaxial tension (b,d) (cf. Section 5.4). For the integration methods (see labels) cf. Section 5.1. GI-X-Y: Gauss integration of order Y with X points, TE: Taylor series expansion (with expansion points), EWI-Y: Equal weights integration with Y points.

thus $\Lambda_2^{\mathrm{n}} = 1$, the largest real part among the integration points is outside the range $[\Lambda_3, \Lambda_1]$, and in fact $> \Lambda_1$. For even n, the corresponding imaginary parts are zero, so that the chain free energy function is evaluated at $\Lambda > \Lambda_1$, and given the extremely steep ascent of the series expansion of ψ near the theoretical locking stretch, this leads to an overestimation of the integral. For the odd EWI methods this analysis is more subtle, since the imaginary part of the integration point with highest real part in non-zero. The underestimation can thus only be explained when considering the complex analytic function representing ψ in the complex plane.

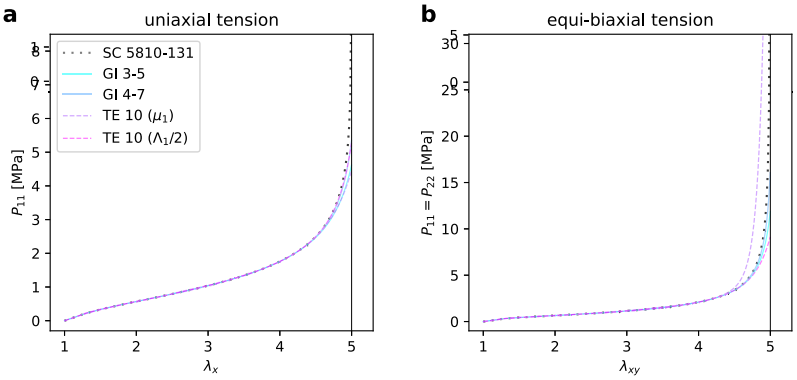

Fig. 5. Full network based on closed form Ilg model [32]. Non-zero components of first Piola–Kirchhoff stress in case of uniaxial (a) and equibiaxial tension (b) (cf. Section 5.4). SC 5810-131: spherical integration ground truth, GI-X-Y: Gauss integration of order Y with X points, TE: Taylor series expansion (with expansion points), cf. Section 5.1.

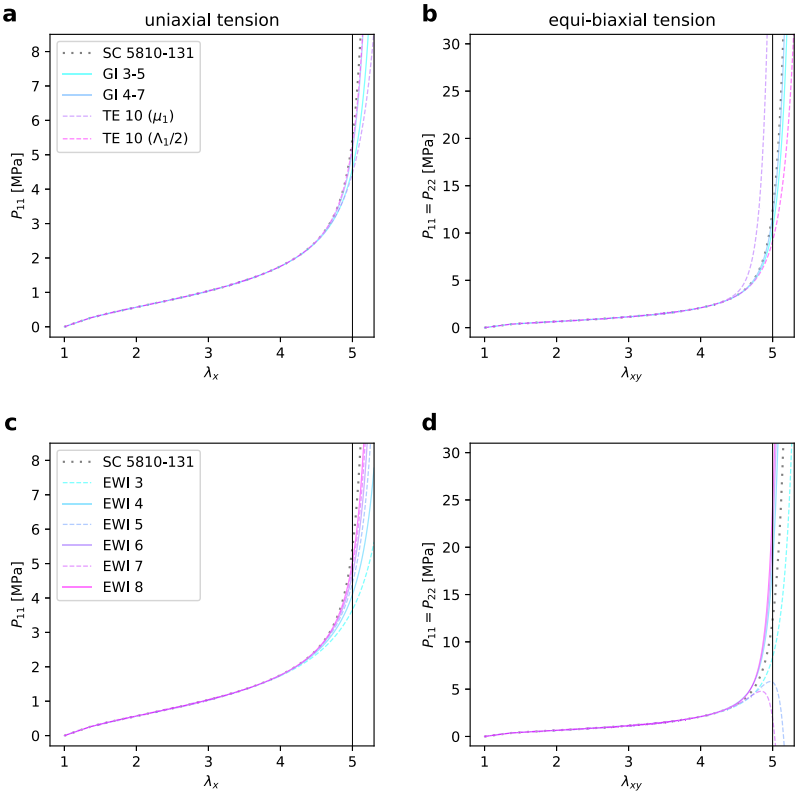

Fig. 6. Full network based on Taylor approximation of Ilg model. Non-zero components of first Piola–Kirchhoff stress in case of uniaxial (a,c) and equibiaxial tension (b,d) (cf. Section 5.4). For the integration methods (see labels) cf. Section 5.1. GI-X-Y: Gauss integration of order Y with X points, TE: Taylor series expansion (with expansion points), EWI-Y: Equal weights integration with Y points.

To this end, Fig. 7a shows the complex continuation of ψ based on a Taylor approximation of the Langevin model for equibiaxial extension, together with the positions of the 5 integration points used to determine $\mathrm{E}[\psi]$ at $\lambda_{xy} = 4.95$ in the EWI 5 method. Since ψ is at a maximum on the real axis ($y = 0$), the evaluation of ψ for $x + iy$ with $y \neq 0$ leads to $\mathrm{Re}(\psi(x + iy)) < \psi(x)$ in the present example. The strong non-linearity of the function for high stretches thus leads to an underestimation of the result. Fig. 7b shows the curves for $\mathrm{Re}(\psi(z_k))$ for all 5 integration points over the whole stretch range of the equibiaxial experiment, and indicates again their position for $\lambda_{xy} = 4.95$.

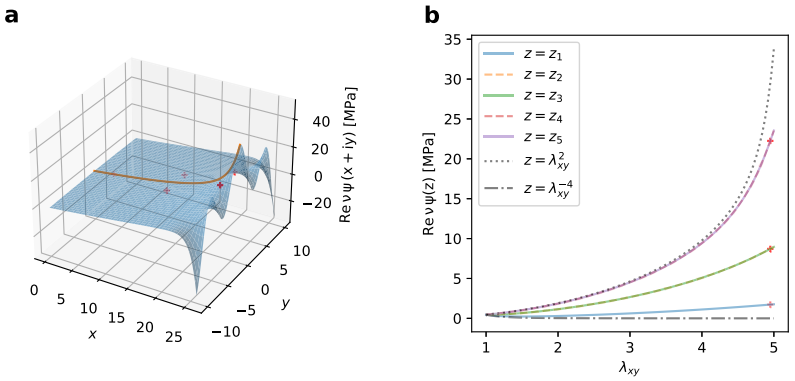

Fig. 7. Complex analytic ψ (Taylor approximation of inv. Langevin model) and integration points of the EWI method: (a) complex continuation (blue surface) of integrand ψ (orange) and location of the integration points (red) of the EWI 5 method for equibiaxial stretch $\lambda_{xy} = 4.95$. (b) evolution of Re(ψ) for the 5 integration points $\{z_k\}$ for equibiaxial tension from $\lambda_{xy} = 1$ to $\lambda_{xy} = 5$. The curves for the minimum and maximum principal stretch are shown as dash-dotted and dotted lines, respectively. (For interpretation of the references to colour in this figure legend, the reader is referred to the web version of this article.)

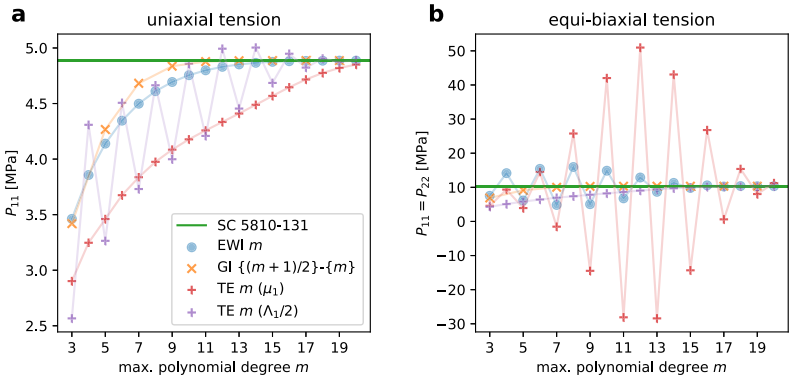

Fig. 8. Convergence study (Full network based on Taylor approximation of inv. Langevin model): (a) uniaxial tension for $\lambda_x = 4.95$ and (b) equibiaxial tension for $\lambda_{xy} = 4.95$. SC 5810-131: ground truth, GI-X-Y: Gauss integration of order Y with X points, TE: Taylor series expansion (with expansion points), EWI-Y: Equal weights integration with Y points.

The Taylor approximation as a polynomial intrinsically fails to capture the asymptotic behaviour of the non-Gaussian chain free energy as the end-to-end stretch approaches the locking value $\lambda \to \sqrt{N}$. Interestingly, however, the overestimation of the series' integral of the even EWI methods (d panels of Figs. 4 and 6) leads to a better approximation of the extensibility limit than the ground truth in equibiaxial tension, although they can clearly not exactly reproduce the asymptotic behaviour.

6.2. Quadrature errors

To investigate the reduction of the integration errors with the use of an increasing number of statistical moments n, we studied the nominal stress close to the extensibility limit, at $\lambda \approx 0.99\,\lambda_{\text{lim}} = 4.95$, for polynomial degrees from $m = 3$ to $m = 20$ (Fig. 8). The Taylor expansion methods (TE) with different expansion points are also added for comparison.

Both proposed methods (GI and EWI) closely approximate the ground truth for large n. For the GI method, the error decreases monotonically and very rapidly. For the EWI method, this monotonicity is observed only when considering the even and odd methods separately, and for $n \geq 7$.

We remind that the GI method needs to compute the weights $\{w_k\}$, and additionally their derivatives with respect to $\mathbf{C}$ when stress and stiffness are required, and is hence slightly more expensive than the EWI method, for which $\{w_k\}$ are constants. In view of accuracy, however, the GI method generally outperforms all other methods in these graphs. Merely the EWI 3 method is more accurate than the GI 2-3 method (both with max. polynomial degree $m = 3$) in both the uniaxial and equibiaxial case. Taking the uni- and equibiaxial cases together, both methods generally lead to smaller errors than the TE method based on the same amount of information through the statistical moments. With increasing accuracy required, the rapid 'convergence' of GI suggests to use the somewhat more expensive Gauss method.

6.3. Comparison with TE method

The here proposed methods share some properties with the TE method, proposed by Itskov et al. [27] and recently discussed in the light of stretch statistical models [9]. In fact, both methods are free of induced anisotropy by construction [cf. e.g. 40], and relate the chain stretch to the macroscopic deformation through the moments of the affine stretch distribution, which are (mixed) polynomials of the principal invariants. While GI and EWI for $n \leq 3$ do not pose restrictions on ψ, EWI with $n > 3$ requires ψ to be complex analytic, the nth order Taylor expansion method TE n needs analytic integrands over the stretch range considered, or functions that are at least $n + 2$ times continuously differentiable if the stiffness tensor is to be continuous. Noteworthy, the new approaches only require the fibre energy to be twice continuously differentiable in order to compute continuous stress and tangent tensors.

Itskov et al. [27] showed that the radius of convergence of the TE method can be adjusted by an appropriate choice of the expansion point, which adds the complexity of defining the latter adequately. While this adaptability might actually be seen as an advantage, it is associated with additional computational cost. For example, we noted that the TE 10 method with $\Lambda_0 = \mu_1$ was much faster than with $\Lambda_0 = \Lambda_1/2$, and this is explained by the need for recalculating the moments with respect to $\Lambda_1/2$ and determining the eigenprojections of $\mathbf{C}$ as well as their derivatives with respect to $\mathbf{C}$ in this case (cf. Section 5.1).

7. Summary and conclusions

In the present work we proposed methods to integrate the free energy ψ of a single fibre or chain towards computing the total strain–energy density $\Psi = \hat{\Psi}(\mathbf{C})$ of a set or network of these elements, changing with macroscopic deformation expressed in $\mathbf{C}$. This problem is typical for what is called the 'structural approach' in biomechanics or 'full network model' in rubber-elasticity. A recently proposed method (GI) based on univariate Gauss quadrature was generalised towards numerically integrating functions up to an arbitrary polynomial degree, and a new, simpler but typically less accurate method (EWI) was proposed that uses a constant set of equal integration weights. The basis for both models is provided by the authors' recent reinterpretation of the averaging operation in terms of the statistics of stretch within the network.

Both methods are relatively straightforward with regard to their implementation and use standard tools of linear algebra, even if the EWI method with $n > 3$ requires complex number operations. We note that the numerical strategies elaborated in the present work may serve as a template to incorporate other moment-based quadrature schemes than Gauss or equal weights-type quadratures elaborated here. Moreover, the moments to inform these approaches are not limited to the isotropic affine moments used here. It is possible to, e.g., employ the moments of affinely deforming anisotropic materials, to which we previously applied a fully analytical version of the GI 3-5 method [14].

Compared to existing methods the approaches have the benefit of not inducing spurious anisotropy by construction, and (when limiting to $n \leq 3$ for EWI) pose little restrictions on the properties of the integrand ψ. In fact, C^m-continuity is sufficient to compute continuous network energy density ($m = 0$), stress ($m = 1$) and tangent tensors ($m = 2$).

We here applied the methods to the affine isotropic full network model of rubber-elasticity based on different implementations of the entropy-elastic constitutive model for the single long chain molecules. Particularly in this application, the mentioned low requirements imposed on the integrand allow applying the GI n and EWI ($n \leq 3$) methods directly to models that reflect limited-chain extensibility, and not to Taylor-series thereof, which clearly lack the asymptotic behaviour intrinsic to these models. When increasing n the GI method approached the ground-truth strikingly fast and actually outperformed the other methods in all test cases considered here. EWI ($n > 3$) includes conjugate complex pairs of integration points and hence requires complex analytic approximations or representations for ψ. However, given that EWI is computationally simpler than the GI method in that it omits the computation of the integration weights, our results indicate that particularly the even-n variants may still be used as effective models to represent the affine full network non-Gaussian chains.

Finally, we note that an additional perspective on the new models can be obtained by consideration of the integration points as the square stretches of a finite set of chains. By this means GI n and EWI ($n \leq 3$) can be interpreted as particular families of n-chain models, i.e. models that evaluate the chain network energy as the sum of free energies provided by n representative chains (see Supplementary Information, Sec. 2).

Altogether, we presented two promising numerical methods to compute averaged constitutive functions of random fibre or chain networks up to arbitrary polynomial accuracy. Although these methods have here been showcased to represent serious alternatives to existing approaches in the particular field of non-Gaussian rubber-elasticity, we anticipate that they may prove useful to address problems beyond this application.

CRediT authorship contribution statement

Ben R. Britt: Conceptualization, Data curation, Formal analysis, Investigation, Methodology, Software, Visualization, Writing – original draft, Writing – review & editing. **Alexander E. Ehret:** Conceptualization, Formal analysis, Funding acquisition, Methodology, Project administration, Supervision, Validation, Writing – review & editing.

Declaration of competing interest

The authors declare that they have no known competing financial interests or personal relationships that could have appeared to influence the work reported in this paper.

Table A.1
Isotropic affine moments.

n	$\tilde{\mu}_n$
0	1
1	0
2	$\frac{4A}{45}$
3	$\frac{16B}{945}$
4	$\frac{16A^2}{945}$
5	$\frac{128AB}{18711}$
6	$\frac{320A^3}{81081} + \frac{512B^2}{729729}$
7	$\frac{256A^2B}{104247}$
8	$\frac{256A\left(63A^3+32B^2\right)}{15949791}$
9	$\frac{4096B\left(189A^3+8B^2\right)}{909138087}$
10	$\frac{1024A^2\left(81A^3+80B^2\right)}{303046029}$
11	$\frac{20480AB\left(243A^3+32B^2\right)}{17108325819}$
12	$\frac{45056A^6}{586705275} + \frac{131072A^3B^2}{1056069495} + \frac{524288B^4}{256624887285}$
13	$\frac{32768A^2B\left(297A^3+80B^2\right)}{98701879725}$
14	$\frac{16384A\left(34749A^6+83160A^3B^2+4480B^4\right)}{25761190608225}$
15	$\frac{458752B\left(34749A^6+15840A^3B^2+128B^4\right)}{479158145312985}$
16	$\frac{65536A^2\left(47385A^6+157248A^3B^2+17920B^4\right)}{479158145312985}$
17	$\frac{2097152AB\left(47385A^6+32760A^3B^2+896B^4\right)}{8878518574917075}$
18	$\frac{57933824A^9}{30041626636665} + \frac{109051904A^6B^2}{12874982844285} + \frac{1744830464A^3B^4}{1042873610387085} + \frac{1073741824B^6}{140787937402256475}$
19	$\frac{1048576A^2B\left(61965A^6+60480A^3B^2+3584B^4\right)}{17289746698522725}$
20	$\frac{1048576A\left(2119203A^9+11897280A^6B^2+3628800A^3B^4+57344B^6\right)}{3827949919052931315}$
21	$\frac{8388608B\left(10596015A^9+13880160A^6B^2+1451520A^3B^4+4096B^6\right)}{70543648508261162805}$
22	$\frac{4194304A^2\left(14834421A^9+1036054480A^6B^2+45239040A^3B^4+1576960B^6\right)}{3527182425413058140 25}$
23	$\frac{184549376AB\left(14834421A^9+25116480A^6B^2+4112640A^3B^4+40960B^6\right)}{64869485476074938840 25}$
24	$\frac{124637937664A^{12}}{2306997908512546725} + \frac{19075023503 36A^9B^2}{4152596235322584105} + \frac{3052003760 5376A^6B^4}{1121200983537097708 35}$ $+ \frac{51402168598528A^3B^6}{3027242655550163812545} + \frac{6047313952768B^8}{1907162872996603201 90335}$
25	$\frac{268435456A^2B\left(20070099A^9+42661080A^6B^2+10112256A^3B^4+225280B^6\right)}{3814325745993206403 8067}$
26	$\frac{67108864A\left(4515772275A^{12}+45920386512A^9B^2+35494018560A^6B^4+3505582080A^3B^6+23429120B^8\right)}{1819433380838759454615 7959}$
27	$\frac{3489660928B\left(406419504 75A^{12}+105970122720A^9B^2+34401894912A^6B^4+1386823680A^3B^6+1802240B^8\right)}{3002065078383953100116 063235}$
28	$\frac{268435456A^2\left(916735725A^{12}+10985738400A^9B^2+107416108 80A^6B^4+1549836288A^3B^6+23429120B^8\right)}{4765182664101512857327 0845}$
29	$\frac{2147483648AB\left(57754350675A^{12}+181264683600A^9B^2+77339598336A^6B^4+4981616640A^3B^6+23429120B^8\right)}{7852692397152113774195 219595}$
30	$\frac{3580928983040A^{15}}{2225555048554239196179} + \frac{642097610 75200A^{12}B^2}{2861427919569736109373} + \frac{5136780886 016000A^9B^4}{1896346321242125112 48447}$ $+ \frac{9205111347740672A^6B^6}{1706711689117912601236023} + \frac{2286984185774080A^3B^8}{1536040520206121341112 4207} + \frac{3659174697238528B^{10}}{2612804924870612401232 2276107}$

Data availability

Data will be made available on request.

Acknowledgement

This work was supported by the Swiss National Science Foundation (SNSF, Project No. 182014).

Appendix A. Moments of the affine distribution

The first 30 central moments $(23)_2$ of the affine stretch distribution for the case of an isotropic orientation distribution are provided in Table A.1. For the first 10, cf. also [27].

Appendix B. 1,2 and 3-point EWI rules

Equal weights quadrature rules with 1,2 or 3 points can be obtained analytically.

The case $n = 1$, i.e. the 1-point integration rule provides an average stretch model [see e.g. 25,49] with $z_1 = \mu_1$. While in the isotropic case this means $z_1 = I_1/3$, we note that for an anisotropic fibre distribution one can set $z_1 = \mu_1 = \mathbf{C} : \mathbb{H}_1$, where $\mathbb{H}_1$ is the first even order structural tensor [see e.g. 9]. In any case, since the stretch random variable is bounded in $[\Lambda_3, \Lambda_1]$ the expectation and therefore z_1 must lie within the same range.

With two integration points ($n = 2$) placed at the negative and positive distance of the standard deviation from the expectation, i.e. $\{z_1, z_2\} = \{\mu_1 - \sqrt{\bar{\mu}_2}, \mu_1 + \sqrt{\bar{\mu}_2}\}$ exact integration of at most quadratic polynomials is possible. For $n = 3$ Eq. (38) becomes the 3-point rule

$$\mathrm{E}[\psi] \approx \mathrm{EWI}[\psi] = \frac{1}{3}\sum_{k=1}^{3} \psi(z_k) \tag{B.1}$$

and Eq. (42) provides the fundamental requirement for the 3 points $\{z_k\}$, i.e.

$$\begin{aligned} &\bar{z}_1 + \bar{z}_2 + \bar{z}_3 = 0 \\ &\bar{z}_1^2 + \bar{z}_2^2 + \bar{z}_3^2 = 3\,\bar{\mu}_2 \\ &\bar{z}_1^3 + \bar{z}_2^3 + \bar{z}_3^3 = 3\,\bar{\mu}_3. \end{aligned} \tag{B.2}$$

Hence in order to determine the relative positions $\{\bar{z}_k\}$ in (B.2) we seek the roots of the characteristic polynomial, i.e. the solutions of

$$\bar{z}_k^3 - I_1 \bar{z}_k^2 + I_2 \bar{z}_k - I_3 = 0, \tag{B.3}$$

where the principal invariants $\{I_l\}$ follow from inserting the values for the main invariants $\{0, 3\,\bar{\mu}_2, 3\,\bar{\mu}_3\}$ into (4). Eq. (B.3) has either three real or one real and two complex conjugate roots. By virtue of Cardano's formula one finds

$$z_k = \mu_1 + \bar{z}_k = \mu_1 + \alpha \cos\left(\frac{\arccos(\beta) + 2\pi(k-1)}{3}\right) =: \mu_1 + \alpha \underbrace{\cos(\gamma_k)}_{C_k}, \tag{B.4}$$

with

$$\alpha = \sqrt{2\,\bar{\mu}_2}, \qquad \beta = \frac{\sqrt{2}\,\bar{\mu}_3}{\bar{\mu}_2^{3/2}}, \tag{B.5}$$

where here and henceforth we assume $\bar{\mu}_2 \neq 0$. We emphasise, that given a *stable* problem, adding a small perturbation to $\bar{\mu}_2$ to enforce this restriction if needed per definition does not significantly affect the result [cf. e.g. 50]. We also note that if $\bar{\mu}_2 = 0$, then all eigenvalues $\{\bar{z}_k\}$ vanish, i.e. $z_k = \mu_1$ for all k, and the problem simplifies to 1-point case. For an affine deformation and uniform fibre orientation distribution, it can be shown that $-1 < \beta < 1$, and thus the values $\{z_i\}$ are real and lie between the minimal and maximal eigenvalue of $\mathbf{C}$ (Supplementary Information, Sec. 1).

The quantities $z_{k,\mathbf{C}}$ and $z_{k,\mathbf{CC}}$ essential for the calculation of stress and stiffness can be determined fully analytically. E.g. for $n = 3$

$$z_{k,\mathbf{C}} = \mu_{1,\mathbf{C}} + C_k\,\alpha_{,\mathbf{C}} + \frac{\alpha S_k}{3\sqrt{1-\beta^2}}\,\beta_{,\mathbf{C}}\,, \tag{B.6}$$

and

$$z_{k,\mathbf{CC}} = \mu_{1,\mathbf{CC}} + C_k\,\alpha_{,\mathbf{CC}} + \frac{S_k}{3\sqrt{1-\beta^2}}\left(\alpha_{,\mathbf{C}} \otimes \beta_{,\mathbf{C}} + \beta_{,\mathbf{C}} \otimes \alpha_{,\mathbf{C}}\right) + \frac{\alpha}{3(1-\beta^2)}\left(\frac{\beta S_k}{\sqrt{1-\beta^2}} - \frac{C_k}{3}\right)\beta_{,\mathbf{C}} \otimes \beta_{,\mathbf{C}} + \frac{\alpha S_k}{3\sqrt{1-\beta^2}}\beta_{,\mathbf{CC}}\,, \tag{B.7}$$

where $C_k = \cos(\gamma_k)$ and $S_k = \sin(\gamma_k)$, γ_k is defined in (B.4) and by the Pythagoras trigonometric identity $C_k^2 + S_k^2 = 1$. It can be seen that these derivatives require $\beta^2 \neq 1$, which is always the case for an isotropic fibre distribution.

Appendix C. Taylor approximation of the model by Ilg et al. [32]

The coefficients C_k up to $n = 34$ specifying the truncated series (83) are given in Table C.2.

Appendix D. Supplementary data

Supplementary material related to this article can be found online at https://doi.org/10.1016/j.cma.2024.116792.

Table C.2
Coefficients for Taylor approximation of model by Ilg et al. [32].

k	C_k
1	$\frac{1}{6}$
2	$\frac{1}{180}$
3	$\frac{1}{2835}$
4	$\frac{1}{37800}$
5	$\frac{1}{467775}$
6	$\frac{691}{3831077250}$
7	$\frac{2}{127702575}$
8	$\frac{3617}{2605132530000}$
9	$\frac{43867}{350813659321125}$
10	$\frac{174611}{15313294652906250}$
11	$\frac{155366}{147926426347074375}$
12	$\frac{236364091}{2423034863565078262500}$
13	$\frac{1315862}{144228265688397515625}$
14	$\frac{3392780147}{3952575621190533915703125}$
15	$\frac{6892673020804}{8491318207003624011050234375}$
16	$\frac{7709321041217}{9998435291363574593162625000000}$
17	$\frac{151628697551}{2062177278843737259839791406 25}$
18	$\frac{263152715530534773 73}{37400359611359859455677731591 6808593750}$
19	$\frac{308420411983322}{4566588475135513975052226079570 3125}$
20	$\frac{2610827184964491220 51}{4016086234457927765359680225678111 32812500}$
21	$\frac{3040195287836141605382}{4846357298619816268196448298515801598242 1875}$
22	$\frac{2530297234481911294093}{4170504750172835087937759930355434708691406 25}$
23	$\frac{1037306281032890718744 28}{1764123509323109242197672450504034888177646484375}$
24	$\frac{5609403368997817686249127547}{9824756648122259991647277411549310992389488007812 5000}$
25	$\frac{3960457641928637185699820 2}{7131469286438669111584090881309360354581359130859375}$
26	$\frac{6162813216426845825753269 1681}{1139057723891674517781606224901498243180156265905761718 75}$
27	$\frac{1165998545395394496856724952507 64}{2208792394707301724411023894955491303280368221468498779296875}$
28	$\frac{3541989899018895362407736770947 47}{6867492923115294835157082090553623057957480142772427978515625 0}$
29	$\frac{1165291218605241956717886565434979 6}{2309537870043673653063326707053183434391100572014367529174804687 5}$
30	$\frac{2430466280967511144080609988159640492082982}{4918166379410444397923280248070683374846505346968454187500628372192382812 5}$
31	$\frac{3174344628151447365665300608362164168}{6551004168378880316914126204556354811650356772518753496504333496093 75}$
32	$\frac{1067838301478665298863854449791426479420 17}{2245160148586809862212809332825553921048810273077627198321965175781250000 0}$
33	$\frac{1338727292842123321865108571410847583856271 91}{2864822079673825040901514897940676924481339671598430627310741025545318603515625}$
34	$\frac{1252355021601251639775980114602140003884 69}{2725195867856025163411434909349868933813596016852628317625348186126708984375 0}$

References

[1] B.R. Britt, A.E. Ehret, Constitutive modelling of fibre networks with stretch distributions. Part I: Theory and illustration, J. Mech. Phys. Solids 167 (2022) 104960, http://dx.doi.org/10.1016/j.jmps.2022.104960.

[2] L.R.G. Treloar, G. Riding, A non-Gaussian theory for rubber in biaxial strain. I. Mechanical properties, Proc. R. Soc. Lond. Ser. A Math. Phys. Eng. Sci. 369 (1737) (1979) 261–280, http://dx.doi.org/10.1098/rspa.1979.0163.

[3] P.D. Wu, E. Van Der Giessen, On improved network models for rubber elasticity and their applications to orientation hardening in glassy polymers, J. Mech. Phys. Solids 41 (3) (1993) 427–456, http://dx.doi.org/10.1016/0022-5096(93)90043-F.

[4] Y. Lanir, Constitutive equations for fibrous connective tissues, J. Biomech. 16 (1) (1983) 1–12, http://dx.doi.org/10.1016/0021-9290(83)90041-6.

[5] K.L. Billiar, M.S. Sacks, Biaxial mechanical properties of the native and glutaraldehyde-treated aortic valve cusp: Part II – A structural constitutive model, J. Biomech. Eng. 122 (4) (2000) 327–335, http://dx.doi.org/10.1115/1.1287158.

[6] M.S. Sacks, Incorporation of experimentally-derived fiber orientation into a structural constitutive model for planar collagenous tissues, J. Biomech. Eng. 125 (2) (2003) 280–287, http://dx.doi.org/10.1115/1.1544508.

[7] S. Federico, W. Herzog, Towards an analytical model of soft biological tissues, J. Biomech. 41 (16) (2008) 3309–3313, http://dx.doi.org/10.1016/j.jbiomech.2008.05.039.

[8] K. Li, R.W. Ogden, G.A. Holzapfel, A discrete fibre dispersion method for excluding fibres under compression in the modelling of fibrous tissues, J. R. Soc. Interface 15 (138) (2018) 20170766, http://dx.doi.org/10.1098/rsif.2017.0766.

[9] B.R. Britt, A.E. Ehret, Constitutive modelling of fibre networks with stretch distributions, Part II: Alternative representation, affine distribution and anisotropy, J. Mech. Phys. Solids 175 (2023) 105291, http://dx.doi.org/10.1016/j.jmps.2023.105291.

[10] A. Gizzi, A. Pandolfi, M. Vasta, Statistical characterization of the anisotropic strain energy in soft materials with distributed fibers, Mech. Mater. 92 (2016) 119–138, http://dx.doi.org/10.1016/j.mechmat.2015.09.008.
[11] M. Vasta, A. Gizzi, A. Pandolfi, A spectral decomposition approach for the mechanical statistical characterization of distributed fiber-reinforced tissues, Int. J. Non-Linear Mech. 106 (2018) 258–265, http://dx.doi.org/10.1016/j.ijnonlinmec.2018.06.010.
[12] W. Gautschi, Moments in quadrature problems, Comput. Math. Appl. 33 (1) (1997) 105–118, http://dx.doi.org/10.1016/S0898-1221(96)00223-4.
[13] W. Gautschi, On generating Gaussian quadrature rules, in: G. Hämmerlin (Ed.), Numerische Integration, in: International Series of Numerical Mathematics / Internationale Schriftenreihe zur Numerischen Mathematik / Série Internationale D'Analyse Numérique, vol. 45, Birkhäuser, Basel, 1979, pp. 147–154, http://dx.doi.org/10.1007/978-3-0348-6288-2_10.
[14] B.R. Britt, A.E. Ehret, Univariate Gauss quadrature for structural modelling of tissues and materials with distributed fibres, Comput. Methods Appl. Mech. Engrg. 415 (2023) 116281, http://dx.doi.org/10.1016/j.cma.2023.116281.
[15] A. Pandolfi, M. Vasta, Fiber distributed hyperelastic modeling of biological tissues, Mech. Mater. 44 (2012) 151–162, http://dx.doi.org/10.1016/j.mechmat.2011.06.004.
[16] D.H. Cortes, D.M. Elliott, Accurate prediction of stress in fibers with distributed orientations using generalized high-order structure tensors, Mech. Mater. 75 (2014) 73–83, http://dx.doi.org/10.1016/j.mechmat.2014.04.006.
[17] K. Hashlamoun, A. Grillo, S. Federico, Efficient evaluation of the material response of tissues reinforced by statistically oriented fibres, Z. Angew. Math. Phys. 67 (5) (2016) 113, http://dx.doi.org/10.1007/s00033-016-0704-5.
[18] M. Kalhöfer-Köchling, E. Bodenschatz, Y. Wang, Structure tensors for dispersed fibers in soft materials, Phys. Rev. A 13 (2020) 064039, http://dx.doi.org/10.1103/PhysRevApplied.13.064039.
[19] K.-I. Kanatani, Stereological determination of structural anisotropy, Internat. J. Engrg. Sci. 22 (5) (1984) 531–546, http://dx.doi.org/10.1016/0020-7225(84)90055-7.
[20] S.G. Advani, C.L. Tucker, The use of tensors to describe and predict fiber orientation in short fiber composites, J. Rheol. 31 (8) (1987) 751–784.
[21] K. Hashlamoun, S. Federico, Transversely isotropic higher-order averaged structure tensors, Z. Angew. Math. Phys. 68 (4) (2017) 88, http://dx.doi.org/10.1007/s00033-017-0830-8.
[22] M. Puso, Mechanistic Constitutive Models for Rubber Elasticity and Viscoelasticity, Technical Report UCRL-ID-151578, Lawrence Livermore National Lab., CA (US), 2003, http://dx.doi.org/10.2172/15004918.
[23] C. Miehe, S. Göktepe, F. Lulei, A micro-macro approach to rubber-like materials – Part I: The non-affine micro-sphere model of rubber elasticity, J. Mech. Phys. Solids 52 (2004) 2617–2660, http://dx.doi.org/10.1016/j.jmps.2004.03.011.
[24] G. Perrin, Analytic stress-strain relationship for isotropic network model of rubber elasticity, C. R. l'Acad. Sci. Ser. IIb Mec. Phys. Chimie Astron. 328 (1) (2000) 5–10, http://dx.doi.org/10.1016/S1287-4620(00)88409-4.
[25] M.F. Beatty, An average-stretch full-network model for rubber elasticity, J. Elasticity 70 (1) (2003) 65–86, http://dx.doi.org/10.1023/B:ELAS.0000005553.38563.91.
[26] J. Diani, P. Gilormini, Combining the logarithmic strain and the full-network model for a better understanding of the hyperelastic behavior of rubber-like materials, J. Mech. Phys. Solids 53 (11) (2005) 2579–2596, http://dx.doi.org/10.1016/j.jmps.2005.04.011.
[27] M. Itskov, A.E. Ehret, R. Dargazany, A full-network rubber elasticity model based on analytical integration, Math. Mech. Solids 15 (6) (2010) 655–671, http://dx.doi.org/10.1177/1081286509106441.
[28] M. Itskov, On the accuracy of numerical integration over the unit sphere applied to full network models, Comput. Mech. 57 (5) (2016) 859–865, http://dx.doi.org/10.1007/s00466-016-1265-3.
[29] L.R.G. Treloar, The Physics of Rubber Elasticity, third ed., Clarendon Press, Oxford, 2005.
[30] M. Klüppel, Finite chain extensibility and topological constraints in swollen networks, Macromolecules 27 (24) (1994) 7179–7184, http://dx.doi.org/10.1021/ma00102a028.
[31] A. Cohen, A Padé approximant to the inverse Langevin function, Rheol. Acta 30 (3) (1991) 270–273, http://dx.doi.org/10.1007/BF00366640.
[32] P. Ilg, I.V. Karlin, S. Succi, Supersymmetry solution for finitely extensible dumbbell model, Europhys. Lett. 51 (3) (2000) 355, http://dx.doi.org/10.1209/epl/i2000-00360-9.
[33] M. Itskov, Tensor Algebra and Tensor Analysis for Engineers: With Applications to Continuum Mechanics, fifth ed., in: Mathematical Engineering, Springer, Cham, 2019, http://dx.doi.org/10.1007/978-3-319-98806-1.
[34] R.A. Horn, C.R. Johnson, Matrix Analysis, second ed., Cambridge University Press, Cambridge, New York, 2012.
[35] X.-M. Niu, T. Sakurai, A method for finding the zeros of polynomials using a companion matrix, Jpn. J. Ind. Appl. Math. 20 (2) (2003) 239, http://dx.doi.org/10.1007/BF03170428.
[36] J. Stoer, R. Bulirsch, Introduction to Numerical Analysis, third ed., Springer, New York, NY, 2002, http://dx.doi.org/10.1007/978-0-387-21738-3.
[37] G. Szegö, Orthogonal Polynomials, in: American Mathematical Society Colloquium Publications, vol. 23, American Mathematical Society, 1939.
[38] B.R. Britt, Supplementary material: Univariate Gauss quadrature for structural modelling of tissues and materials with distributed fibres, ETH Res. Collect. (2023) http://dx.doi.org/10.3929/ethz-b-000620418.
[39] P. Bažant, B.H. Oh, Efficient numerical integration on the surface of a sphere, ZAMM Z. Angew. Math. Mech. 66 (1) (1986) 37–49, http://dx.doi.org/10.1002/zamm.19860660108.
[40] A.E. Ehret, M. Itskov, H. Schmid, Numerical integration on the sphere and its effect on the material symmetry of constitutive equations – A comparative study, Internat. J. Numer. Methods Engrg. 81 (2) (2010) 189–206, http://dx.doi.org/10.1002/nme.2688.
[41] V.I. Lebedev, Quadratures on a sphere, USSR Comput. Math. Math. Phys. 16 (2) (1976) 10–24, http://dx.doi.org/10.1016/0041-5553(76)90100-2.
[42] J. Burkardt, Sphere lebedev rule - Quadrature rules for the sphere, 2010, John Burkardt, https://people.sc.fsu.edu/~jburkardt/datasets/sphere_lebedev_rule/sphere_lebedev_rule.html. [Accessed 24 November 2022].
[43] W. Kuhn, F. Grün, Beziehungen zwischen elastischen Konstanten und Dehnungsdoppelbrechung hochelastischer Stoffe, Kolloid-Zeitschrift 101 (3) (1942) 248–271, http://dx.doi.org/10.1007/BF01793684.
[44] M. Itskov, R. Dargazany, K. Hörnes, Taylor expansion of the inverse function with application to the Langevin function, Math. Mech. Solids 17 (7) (2012) 693–701, http://dx.doi.org/10.1177/1081286511429886.
[45] V.N. Khiêm, M. Itskov, Analytical network-averaging of the tube model: Rubber elasticity, J. Mech. Phys. Solids 95 (2016) 254–269, http://dx.doi.org/10.1016/j.jmps.2016.05.030.
[46] V.N. Khiêm, M. Itskov, An averaging based tube model for deformation induced anisotropic stress softening of filled elastomers, Int. J. Plast. 90 (2017) 96–115, http://dx.doi.org/10.1016/j.ijplas.2016.12.007.
[47] A.E. Ehret, A. Stracuzzi, Variations on Ogden's model: Close and distant relatives, Phil. Trans. R. Soc. A 380 (2234) (2022) 20210322, http://dx.doi.org/10.1098/rsta.2021.0322.
[48] R.W. Ogden, Non-Linear Elastic Deformations, E. Horwood, Mineola, NY, 1997, Republication of 1984 edition.
[49] A.E. Ehret, On a molecular statistical basis for Ogden's model of rubber elasticity, J. Mech. Phys. Solids 78 (2015) 249–268, http://dx.doi.org/10.1016/j.jmps.2015.02.006.
[50] C. Miehe, Comparison of two algorithms for the computation of fourth-order isotropic tensor functions, Comput. Struct. 66 (1) (1998) 37–43, http://dx.doi.org/10.1016/S0045-7949(97)00073-4.